Article

Cell

ASICs Mediate Food Responses in an Enteric Serotonergic Neuron that Controls Foraging Behaviors

Graphical Abstract

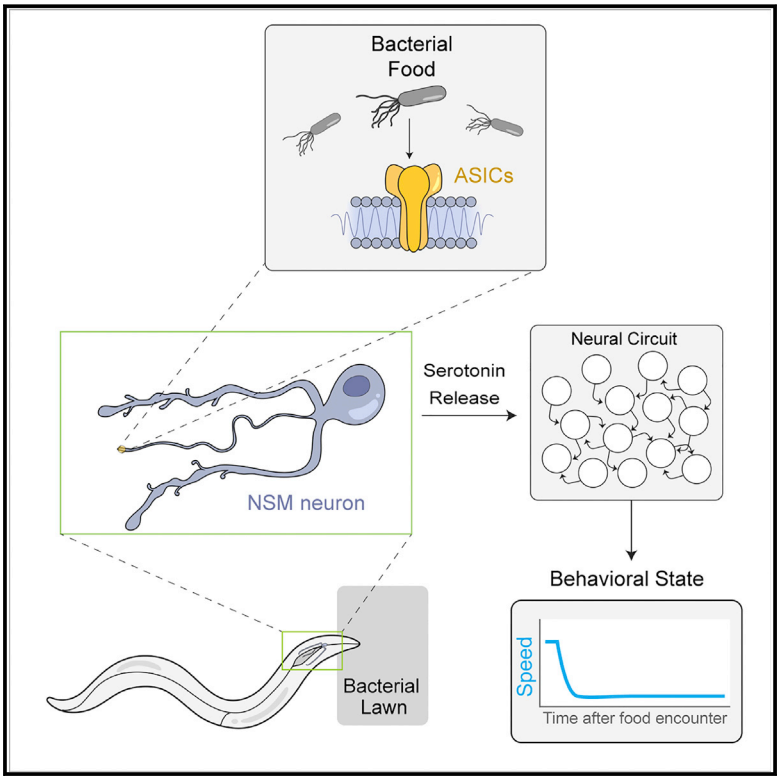

Highlights

- NSM is an enteric serotonergic neuron that is activated by food ingestion
- Two ASIC channels, DEL-7 and DEL-3, mediate feeding-induced NSM activation
- Activation of NSM neurons drives slow locomotion while animals feed
- Changes in NSM response dynamics alter foraging behavior dynamics

Authors

Jeffrey L. Rhoades, Jessica C. Nelson, Ijeoma Nwabudike, ..., Joshua R. Powers, Daniel A. Colón-Ramos, Steven W. Flavell

Correspondence

flavell@mit.edu

In Brief

A sensory mechanism for food sensing and feeding-associated behaviors is mediated by two ASIC ion channels.

Rhoades et al., 2019, Cell *176*, 85–97
January 10, 2019
https://doi.org/10.1016/j.cell.2018.11.023

CellPress

Article

Cell

ASICs Mediate Food Responses in an Enteric Serotonergic Neuron that Controls Foraging Behaviors

Jeffrey L. Rhoades,[1] Jessica C. Nelson,[2] Ijeoma Nwabudike,[1] Stephanie K. Yu,[1] Ian G. McLachlan,[1] Gurrein K. Madan,[1] Eden Abebe,[1] Joshua R. Powers,[1] Daniel A. Colón-Ramos,[2] and Steven W. Flavell[1,3,*]

[1]Picower Institute for Learning and Memory, Department of Brain and Cognitive Sciences, Massachusetts Institute of Technology, Cambridge, MA 02139, USA

[2]Department of Neuroscience and Department of Cell Biology, Program in Cellular Neuroscience, Neurodegeneration, and Repair, Yale University School of Medicine, New Haven, CT 06536, USA

[3]Lead Contact

*Correspondence: flavell@mit.edu

https://doi.org/10.1016/j.cell.2018.11.023

SUMMARY

Animals must respond to the ingestion of food by generating adaptive behaviors, but the role of gut-brain signaling in behavioral regulation is poorly understood. Here, we identify conserved ion channels in an enteric serotonergic neuron that mediate its responses to food ingestion and decipher how these responses drive changes in foraging behavior. We show that the *C. elegans* serotonergic neuron NSM acts as an enteric sensory neuron that acutely detects food ingestion. We identify the novel and conserved acid-sensing ion channels (ASICs) DEL-7 and DEL-3 as NSM-enriched channels required for feeding-dependent NSM activity, which in turn drives slow locomotion while animals feed. Point mutations that alter the DEL-7 channel change NSM dynamics and associated behavioral dynamics of the organism. This study provides causal links between food ingestion, molecular and physiological properties of an enteric serotonergic neuron, and adaptive feeding behaviors, yielding a new view of how enteric neurons control behavior.

INTRODUCTION

All animals must respond to the ingestion of food by generating adaptive behaviors. Enteroendocrine cells and neurons of the enteric nervous system line the gastrointestinal (GI) tract and play crucial roles in mediating responses to food ingestion. These cells have sensory roles in detecting the contents of the alimentary canal (Bellono et al., 2017) and regulate local processes like GI motility and secretion (Mawe and Hoffman, 2013). They can also signal to the CNS via action on vagal sensory neurons that innervate the gut. It is widely thought that gut-brain signaling might be important for the regulation of internal states like mood and appetite, but we currently have a poor understanding of how enteric neurons detect feeding cues and generate neural activity patterns that influence CNS circuits and complex behaviors.

Enteroendocrine cells and enteric neurons signal in large part through hormones and neuromodulators: they produce >90% of the serotonin (5-HT) found in the body, as well as other biogenic amines and neuropeptides. The role of 5-HT has received particular interest, due to its importance for human health. It is well known that 5-HT has local effects in the gut and that vagal afferent neurons express 5-HT receptors that should allow for signal propagation to the CNS (Mawe and Hoffman, 2013). However, it is not known how patterned 5-HT release in the gut influences behavior. Even within the CNS, the function of 5-HT is poorly understood. There are many molecularly distinct subtypes of 5-HTergic neurons in the dorsal raphe nucleus (Okaty et al., 2015). Neural recordings from this heterogeneous population have revealed diverse activity profiles, reflecting rewarding stimuli like food (Li et al., 2016), and complex cognitive processes (Cohen et al., 2015). Optogenetic stimulation of 5-HTergic neurons in rodents can elicit many behavioral effects, including slow locomotion, waiting/perseverance, and changes in reward learning (Correia et al., 2017; Liu et al., 2014). Overall, the causal links between the molecular profiles of 5-HTergic neuron subtypes, their activity patterns, and the behaviors induced by these activity patterns remain enigmatic for this important modulatory system, both in the CNS and in gut-brain signaling.

In the well-defined nervous system of *C. elegans*, neuromodulators like 5-HT are known to regulate behaviors associated with feeding. Acute exposure to food alters animals' locomotion, egg-laying, and pharyngeal pumping, and these effects require monoamines like 5-HT and dopamine, as well as neuropeptides (Li and Kim, 2008; Sawin et al., 2000; Waggoner et al., 1998). For example, the egg-laying events that *C. elegans* display while feeding require 5-HTergic HSN neurons (Waggoner et al., 1998). We previously characterized how *C. elegans* locomotion is altered by the presence of food. While exploring food patches, *C. elegans* switch between two persistent behavioral states: dwelling states where they restrict their movement to a small area, and roaming states where they explore a large area (Ben Arous et al., 2009; Flavell et al., 2013; Fujiwara et al., 2002).

Each state can last minutes, and the proportion of time spent in each state is influenced by food density, so that animals dwell more in favorable food environments. We previously found that neuromodulators stabilize these states: stable dwelling states require 5-HT, and stable roaming states require the neuropeptide pigment dispersing factor (Flavell et al., 2013). This role of neuromodulation in driving persistent behavioral states has been observed for other *C. elegans* behaviors (Choi et al., 2013) and in other animals (Saper et al., 2010).

We previously identified the 5-HTergic neuron NSM as a key regulator of feeding-related dwelling states (Flavell et al., 2013). Indeed, this neuron is required for feeding-dependent switches to slow locomotion in several contexts (Iwanir et al., 2016; Sawin et al., 2000). NSM extends a synapse-less neurite into the alimentary canal (Axäng et al., 2008), suggesting a potential role in food sensation, but specific hypotheses and molecular mechanisms for NSM function remain unexplored.

Here, we show that NSM acts as an enteric sensory neuron that acutely detects food ingestion through a mechanism that requires DEL-3 and DEL-7, two previously uncharacterized ion channels in the evolutionarily conserved ASIC family. These channels localize to NSM sensory endings in the alimentary canal and are required for feeding-dependent NSM activity, which in turn drives slow locomotion while animals feed. Point mutations that alter the DEL-7 channel alter NSM's dynamical response to food ingestion and associated behavioral dynamics. This study identifies a molecular mechanism for bacterial detection by enteric neurons and illustrates how activity in enteric neurons can control behavioral responses to food ingestion.

RESULTS

NSM Is an Enteric Serotonergic Neuron that Senses Acute Food Ingestion

We and others have shown that NSM activation drives slow locomotion via its release of 5-HT (Flavell et al., 2013; Iwanir et al., 2016; Sawin et al., 2000). However, the mechanisms that drive endogenous NSM activity were unclear. The unique anatomy of NSM suggests that it might be involved in gut-brain signaling. NSM has one minor neurite (Figure 1A, arrowheads) that, based on electron microscopy (EM) studies, lacks synapses and extends into the alimentary canal (Albertson and Thomson, 1976; Axäng et al., 2008). This neurite is rich in F-actin (Figure S1A) and might act as a sensory dendrite. NSM also has two major neurites (Figure 1A) with 5-HT release sites apposed to pseudocoelemic space that is in contact with the main neuropil of the *C. elegans* nervous system, the nerve ring (Axäng et al., 2008; Nelson and Colón-Ramos, 2013). Given its anatomy and position, we hypothesized that NSM might act as an enteric sensory neuron that directly detects food ingestion and alters behavior via 5-HTergic signaling to downstream circuits.

When *C. elegans* are exposed to food (*E. coli* strain OP50), NSM displays calcium peaks that correlate with transitions to slow locomotion (Flavell et al., 2013). To test whether NSM calcium transients induced by food availability require synaptic input onto NSM, we examined NSM activity in *unc-13(s69)* mutants that display a dramatic deficit in synaptic transmission. NSM makes no electrical synapses in the *C. elegans* connectome. Through *in vivo* calcium imaging of NSM, we observed robust spontaneous NSM activity in feeding *unc-13* animals, but this activity was absent when animals were removed from bacterial food (Figures 1B and 1C; additional controls in Figures S1B and S1C). *unc-31* mutants that are defective in neuropeptide release also display robust NSM calcium transients in feeding animals, but no activity in the absence of food (Figure 1C). Finally, mutations in *aex-2* or *aex-6,* which disrupt intestine-to-neuron neuropeptide signaling, also had no effect on NSM activity (Figure S1D). These data suggest that even with attenuated synaptic and neuropeptidergic inputs, NSM still responds to food availability by generating calcium transients.

Food is a complex stimulus, providing olfactory and mechanosensory cues, proprioceptive cues associated with eating, and post-ingestive cues. We next examined which aspects of food availability are required for NSM activation. First, we noted that NSM was inactive in *unc-31* mutants removed from food (Figure 1C), even though these mutants exhibit robust pharyngeal pumping in the absence of food (Avery et al., 1993). Thus, the motor act of pharyngeal pumping is insufficient to drive NSM activity in the absence of food. We then treated the bacterial food with aztreonam, which prevents bacterial division and results in *E. coli* that are too large to consume (Ben Arous et al., 2009). NSM activity was absent when animals were exposed to aztreonam-treated OP50 (Figure 1C), suggesting that successful ingestion of bacteria is necessary for NSM to display feeding-dependent activity.

To test which features of the ingested bacterial food are critical for NSM activation, we heat-killed bacteria (at 95°C) and examined NSM responses when animals ingested the crude extract or the supernatant after pelleting high density components, like cell membranes. We found that NSM was activated by heat-killed bacteria, but not by the isolated supernatant (Figure 1C). To test for pure mechanical responses, we fed animals bacteria-sized nanobeads (at low pH; see below) and found that this failed to activate NSM (Figure 1C). These data suggest that a heat-insensitive component of bacterial membranes is necessary to drive NSM activation, but pure mechanical cues do not drive NSM activation.

To examine the latency of NSM's response to food ingestion, we devised an optogenetic strategy to control food intake. We expressed the red-shifted opsin Chrimson (Klapoetke et al., 2014) throughout the pharyngeal muscle and found that exposure to red light contracts the pharyngeal muscles of these transgenic animals, halting the rhythmic pumping required for food ingestion (Figure 1D). This effect occurs immediately upon red light exposure, can be sustained for hours, and is rapidly reversible (<5 s) when red light is turned off. Using this tool, we examined NSM calcium transients in feeding animals while red light was turned on and off to control food ingestion. NSM activity was abolished within 30 s after pumping stopped and resumed within 30 s after pumping resumed (Figures 1D and 1E). These data indicate that NSM can detect food within seconds of ingestion, suggesting a fairly direct mode of food sensing. Taken together, these data indicate that NSM acutely responds to the ingestion of bacterial food in a manner that does not require synaptic or neuropeptidergic inputs.

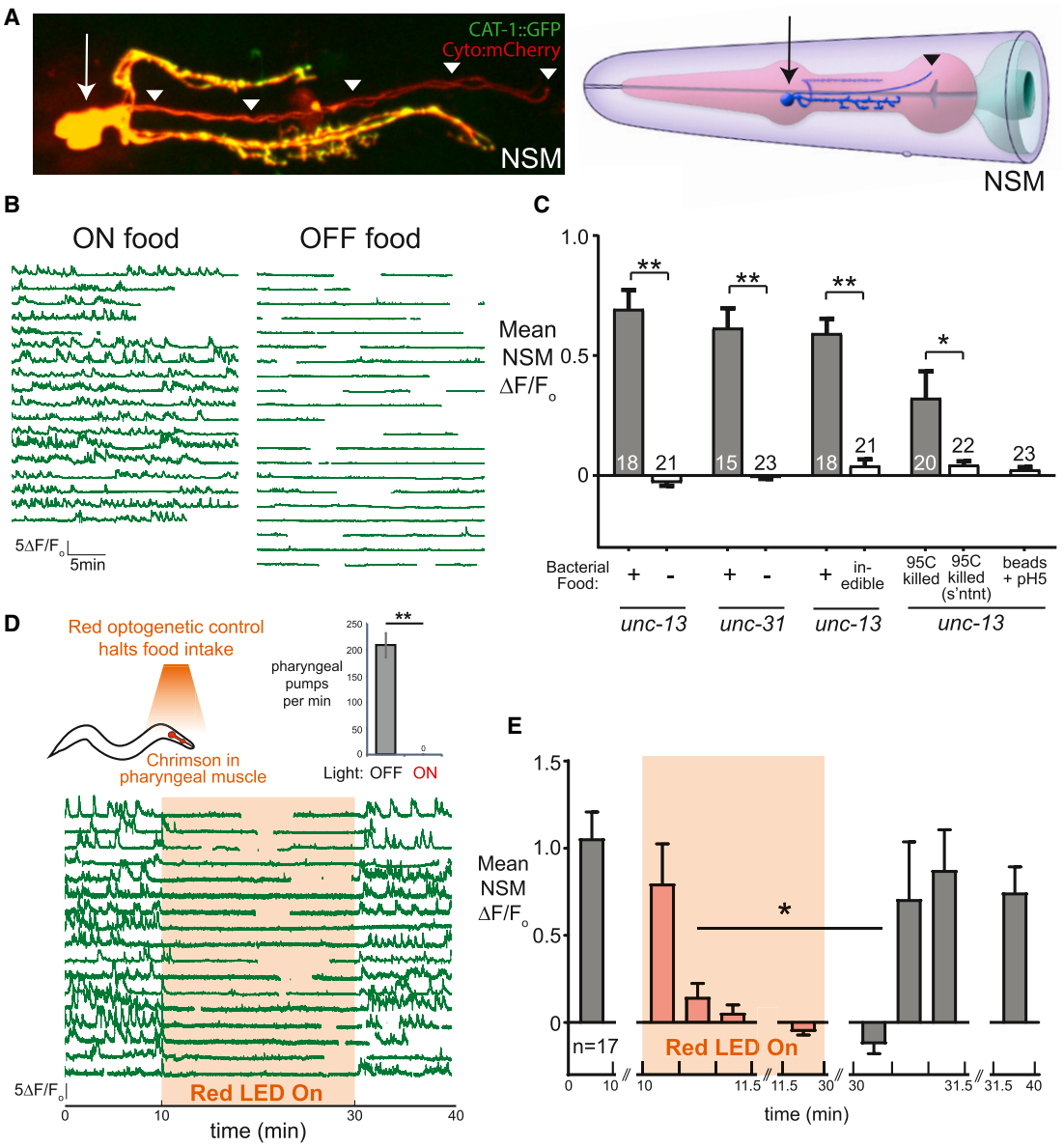

Figure 1. The Serotonergic Neuron NSM Detects Acute Food Ingestion

(A) Left: Confocal image of NSM neurons with soma, axons (yellow) and minor neurite (red) of NSM labeled via CAT-1::GFP (5-HT vesicle marker) and cytoplasmic-mCherry. Synaptic vesicles labeled via CAT-1::GFP are not found in the minor neurite. Right: Cartoon depicting location of NSM in pharynx, reprinted from WormAtlas (http://wormatlas.org) with permission. Arrows mark NSM soma; arrowheads mark minor neurite.

(B) NSM GCaMP traces from *unc-13*(*s69*) animals in the presence or absence of bacterial food. Each line is a recording from one animal. Gaps are due to the *unc-13* animals adopting body postures that obscured NSM GCaMP.

(C) Average NSM GCaMP signals across animals for indicated conditions. "Inedible" is animals exposed to aztreonam-treated *E. coli*. "s'ntnt" refers to bacterial supernatant. **p < 0.001, t test; *p < 0.05, t test.

(D) Top: Optogenetic strategy to control food intake with *myo-2::Chrimson*, and pharyngeal pumping in these animals in the absence or presence of red light (**p < 0.001, paired t test; n = 6 animals). Bottom: NSM calcium traces from *unc-13*(*s69*);*myo-2::Chrimson* animals.

(E) Average NSM GCaMP signals for data in (D), shown for the indicated time bins. n = 17 animals. *p < 0.01 versus 0–10 min time period, ANOVA and Dunnett's test.

Where applicable, n is indicated in bars. Data are shown as means ± SEM. See also Figure S1.

The ASICs DEL-7 and DEL-3 Are Enriched in NSM Neurons

To clarify how NSM is activated by acute food ingestion, we sought to identify receptors and channels in NSM that are required for its feeding-dependent activity. We performed molecular profiling of NSM neurons from feeding, adult animals using tagged ribosome affinity purification (TRAP) (Heiman et al., 2008; Sanz et al., 2009). We expressed an HA-tagged *rpl-22*

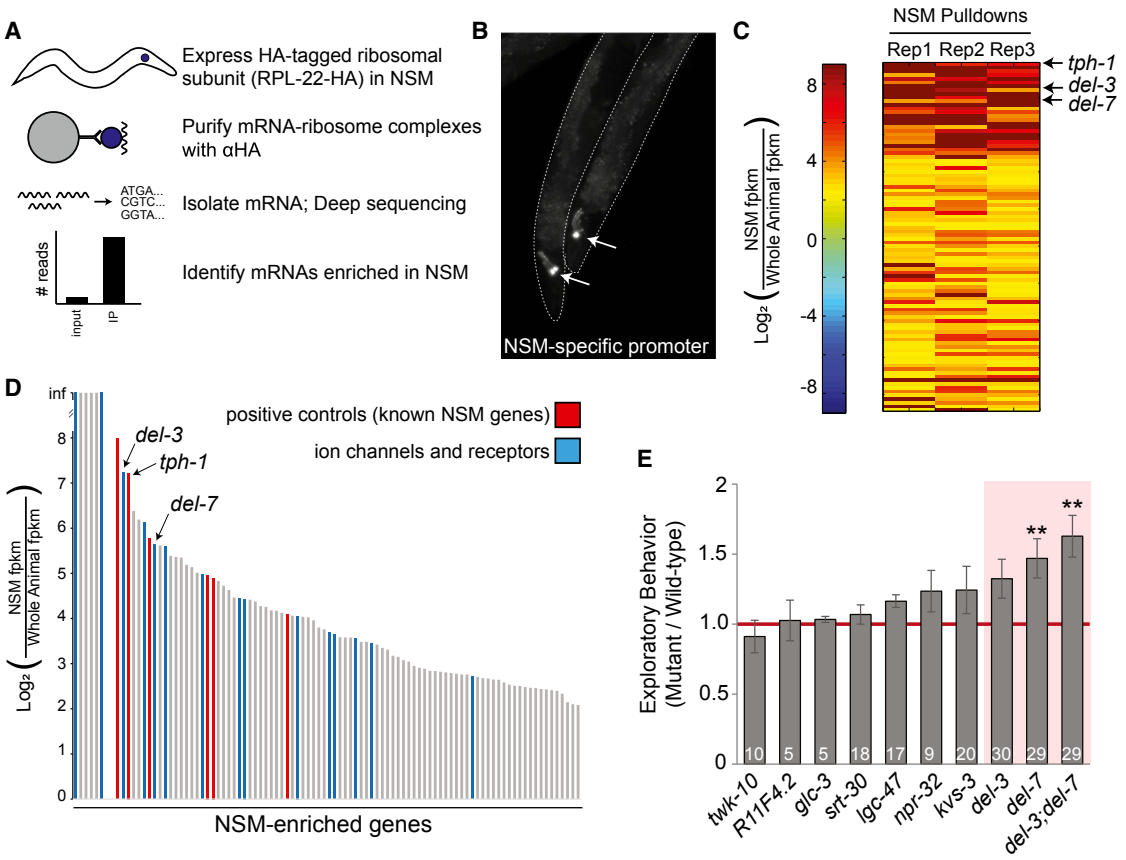

Figure 2. Identification of *del-3* and *del-7* as NSM-Enriched Ion Channels

(A) Cartoon depicting NSM TRAP.

(B) Image of two NSM::rpl-22-3xHA animals, co-expressing GFP under same NSM-specific promoter. GFP-positive NSM neurons indicated by arrows.

(C) Heatmap showing NSM enrichment for 94 genes identified through NSM TRAP. Data are shown for each biological replicate and are sorted based on hierarchical clustering.

(D) Average NSM enrichment of TRAP-identified genes. Red indicates genes with previously known NSM enrichment. Blue indicates genes with predicted transmembrane domains.

(E) Exploratory behavior of mutants lacking NSM-enriched receptors or channels, normalized to WT. A value of 1.0 (red line) indicates no change from WT. Data are shown as means ± SEM. **$p < 0.01$, Bonferroni-corrected t test. n is indicated in bars.

See also Figure S2 and Table S1.

cDNA in NSM, purified the HA-tagged mRNA-ribosome complexes from adult animals, and subjected the isolated RNA to mRNA-seq, along with whole animal RNA for normalization (Figures 2A and 2B).

We performed three independent biological replicates of NSM TRAP and found a high level of reproducibility among replicates (Figures 2C and S2A). Genes known to have enriched expression in NSM, like those involved in 5-HT signaling (*tph-1*, *cat-1*, *mod-5*) and NSM development (*ceh-2*, *unc-86*), were among the top NSM-enriched genes in our genome-wide dataset (Figure 2D; Table S1). We were able to validate the mRNA-seq results using gene-specific qRT-PCR, both for positive controls and for newly discovered NSM-enriched genes (Figure S2B). These data suggest that single neuron TRAP reliably isolates NSM-enriched mRNAs.

We inspected all of the genes that were enriched in NSM >4-fold in all three replicates (Table S1). Out of 94 total genes, 16 encoded putative receptors or channels (Figure 2D). To determine which of these genes are required for feeding-dependent NSM activity and resulting locomotion changes, we performed a behavioral screen of mutant animals lacking these genes using an NSM-dependent exploration assay that measures the extent to which animals explore a bacterial food lawn (Flavell et al., 2013). We tested mutants for nine of the 16 genes and observed significantly increased exploration in mutants lacking *del-7*, which is predicted to encode a DEG/ENaC superfamily ion channel (Figure 2E). Mutants lacking *del-3*, which is a *del-7* paralog also identified through NSM TRAP, displayed a modest increase in exploration (Figure 2E). Loss of both *del-3* and *del-7* resulted in a strong increase in exploration (Figure 2E). Importantly, *del-3;del-7* mutants had normal food ingestion rates (Figures S3A and S3B). These data indicate that *del-3* and *del-7* are NSM-enriched genes that suppress exploration, a phenotype that is consistent with the possibility that these genes promote NSM activation.

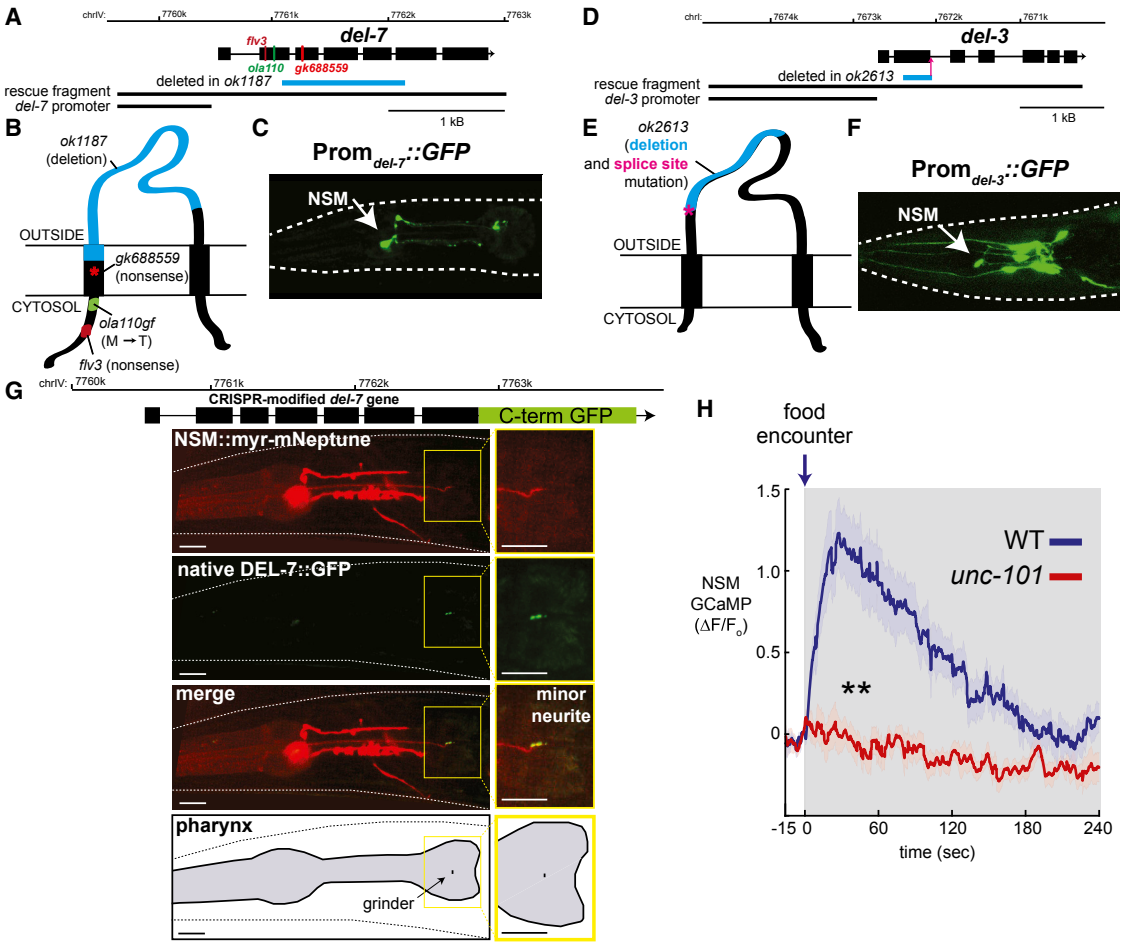

Figure 3. *del-3* and *del-7* Encode NSM-Enriched ASICs

(A) *del-7* genomic region. Boxes indicate exons and lines indicate introns. Mutations used in the study are shown. Genomic regions for rescue fragments and promoters are also shown.

(B) Predicted DEL-7 protein structure, typical of DEG/ENaC subunits. Mutations used in the study are shown.

(C) Example animal expressing *del-7::GFP* transcriptional reporter. The head region is shown and only NSM is detected. Arrow indicates NSM soma.

(D and E) Genomic region (D) and predicted protein (E) for *del-3*, shown as in (A) and (B). The *del-3(ok2613)* deletion (blue) removes most of exon 2, including the splice donor site. This most likely causes ectopic splicing and early termination.

(F) The *del-3::GFP* reporter is expressed in NSM and ~8 other pairs of neurons.

(G) Top: Cartoon depicting *del-7* gene, modified by Cas9/CRISPR so that an in-frame GFP is fused to the DEL-7 C terminus. Bottom: Images of the resulting strain, with NSM::myristoylated-mNeptune to label NSM morphology, DEL-7::GFP, merged images, and outline of the pharynx. Detail on the right shows posterior end of NSM minor neurite. Scale bars, 10 μm.

(H) Average NSM GCaMP signal during food patch encounter in starved WT animals or *unc-101* mutants lacking NSM minor neurite. n = 20 and 15 animals for WT and *unc-101*, respectively. **p < 0.001, t test. Data are means ± SEM.

See also Figure S3.

The genes *del-3* and *del-7* are predicted to encode DEG/ENaC superfamily sodium channels. *del-7* encodes a DEG/ENaC subunit most closely related to ppk13 in *Drosophila* and ASIC1 in mammals (Figures 3A–3C). *del-3* encodes a related channel subunit (Figures 3D–3F). ASICs form homomeric and heteromeric trimers that are permeable to sodium and occasionally calcium ions (Wemmie et al., 2013). In mammals, ASICs are expressed in the CNS and in peripheral sensory neurons; they are known to be involved in pain and GI function (Holzer, 2015; Wemmie et al., 2013). Many distinct activation mechanisms have been described for ASICs, including low pH, small molecules, peptides, and mechanical stimuli. DEL-7 and DEL-3, like most other *C. elegans* ASICs, have not been characterized before.

To determine the *del-3* and *del-7* expression patterns, we fused the promoter sequences for each of these genes to GFP and generated transgenic animals. We observed strong *del-7::GFP* expression exclusively in NSM neurons (Figure 3C). For *del-3::GFP*, we observed expression in NSM and ~8 other pairs of head neurons that we have not yet identified (Figure 3F). Although we cannot rule out additional sites of expression conferred by distal regulatory elements, these results are

consistent with our TRAP data and confirm that *del-7* and *del-3* encode NSM-enriched ion channels.

To examine the subcellular localization of these channels in NSM, we used CRISPR/Cas9 to modify the endogenous *del-7* gene, adding an in-frame flexible linker followed by GFP to the DEL-7 C terminus (Figure 3G). This strain displays normal exploratory behavior, suggesting that addition of GFP does not disrupt *del-7* function (Figure S3C). The DEL-7::GFP channels localized exclusively to the posterior end of the NSM minor neurite, with faint or undetectable signal in the soma and major neurites of NSM (Figure 3G; additional examples in Figure S3D). The posterior end of the NSM minor neurite is located in the alimentary canal in close proximity to the grinder of the pharynx that mechanically lyses bacteria, suggesting that these channels are well-positioned to detect components of lysed bacteria.

Given the exclusive localization of DEL-7 channels in the NSM minor neurite, we examined whether the minor neurite might be involved in mediating feeding-induced NSM activation. We examined mutants lacking the *unc-101* gene, which is required for formation of the NSM minor neurite, but not the other NSM neurites (Axäng et al., 2008). We measured NSM calcium levels in starved *unc-101* mutants as they encountered a food patch (Figure 3H). In contrast to wild-type (WT) animals that display robust NSM calcium peaks upon food encounter (Iwanir et al., 2016), food-deprived *unc-101* animals displayed no NSM response when they encountered food (Figure 3H), despite having robust pharyngeal pumping rates (Figure S3E). These data are consistent with the possibility that NSM's minor neurite detects bacterial food cues in the alimentary canal. Taken together, these data suggest that DEL-7 and DEL-3 are NSM-enriched ASICs that are well-positioned to participate in the detection of bacterial food cues.

del-3 and *del-7* Function in NSM to Promote Slow Locomotion in Response to Food Ingestion

NSM plays an important role in driving abrupt transitions to slow locomotion when animals encounter food patches (Iwanir et al., 2016; Sawin et al., 2000). In WT animals, this transition to slow locomotion occurs immediately upon food encounter and persists for many minutes (Figure 4C), although some animals resume high speed locomotion 1–2 min after food encounter (Figure S4A). We characterized the functions of DEL-3 and DEL-7 during this behavior to specifically examine how these channels contribute to an NSM-dependent behavior that is acutely triggered by food (Figures 4A–4C). Relevant to these ASICs, pH was not detectably altered on or near the bacterial lawn (Figure S4B).

It was not known whether food encounter-induced slowing in *C. elegans* is driven by food ingestion, changes in sensory cues like odors/gases, or both. Thus, we first examined the importance of food ingestion for food patch-induced slowing by optogenetically inhibiting food intake while animals encountered food. This caused a strong, albeit partial, attenuation of the behavioral slowing response (Figure S4C), indicating that both food ingestion and other food sensory cues contribute to this behavioral effect. A previous study showed that inhibiting NSM synaptic vesicle release also causes a partial attenuation of the behavioral slowing response to food (Iwanir et al., 2016). To confirm these results in a temporally precise manner, we silenced NSM during food encounters using a chemogenetic approach (Pokala et al., 2014) and also observed a strong, though partial, attenuation of behavioral slowing (Figure S4D). Thus, food ingestion and NSM neurons play important roles in driving behavioral slowing in response to food, but they do not explain the entire behavioral response.

To assess the roles of *del-3* and *del-7*, we examined the behavioral phenotypes of each single mutant and *del-3;del-7* double mutants. We found that each single mutant had elevated speed at all time points after the food encounter, as did the *del-3;del-7* double mutants, whose phenotype was slightly more severe than each single mutant ($p < 0.01$, ANOVA and Bonferroni-corrected t test, *del-3;del-7* versus single mutants; Figures 4D, S4E, and S4F). Thus, *del-3* and *del-7* are critical for the initial slowing response to food encounter and for persistent slowing minutes later. To verify these effects were specifically due to the loss of the *del-3* and *del-7* genes, we performed genetic rescues. Restoring expression of each gene in the respective single mutants or both genes in the double mutant fully rescued the behavioral defects (Figure 4E). A similar phenotype was also observed for a second, independent loss-of-function allele of *del-7* (Figure S4G). These data indicate that *del-3* and *del-7* play important roles in driving feeding-induced behavioral slowing.

To determine if *del-3* and *del-7* function specifically in NSM to promote behavioral slowing, we expressed both cDNAs under an NSM-specific promoter in double mutant animals. This fully rescued the post-food-encounter speed defects in these mutant animals (Figure 4E). We note that the *del-3;del-7* mutants also display elevated speed immediately before encountering food, though not when they are far away from a food patch (Figures 4D and S4F). Pre-food-encounter speed changes likely reflect sensory detection of nearby food cues (Iwanir et al., 2016). The pre-food-encounter speed defect was fully rescued by transgenic expression from full genomic fragments encompassing both genes, but not by NSM-specific expression of these genes (Figure S4H; similar analysis of *del-7* single mutant in Figure S4I). This indicates that *del-3* and *del-7* function in other cells to promote slow locomotion as animals approach a food patch, but they are specifically required in NSM for post-food encounter slowing. These channels represent the first identified molecular mechanism linking food ingestion to 5-HT-dependent slowing.

NSM Calcium Responses Integrate Acute Food Ingestion with Satiety Levels

We next sought to determine how *del-3* and *del-7* contribute to feeding-dependent NSM activity. Previous work has suggested that NSM has a stronger impact on locomotion in starved animals (Sawin et al., 2000). Thus, we first examined how satiety alters NSM's response to food ingestion and associated behavioral slowing (Figures 5A–5D). Then, we used this information to examine how *del-7* and *del-3* contribute to NSM activity across satiety states (see below).

We examined NSM activity and behavior as WT animals encountered food patches, comparing well-fed animals ("fed") to those that had been deprived of food for 30 min ("fasted") or 3 hr ("starved"). Fasted and starved animals displayed reliable

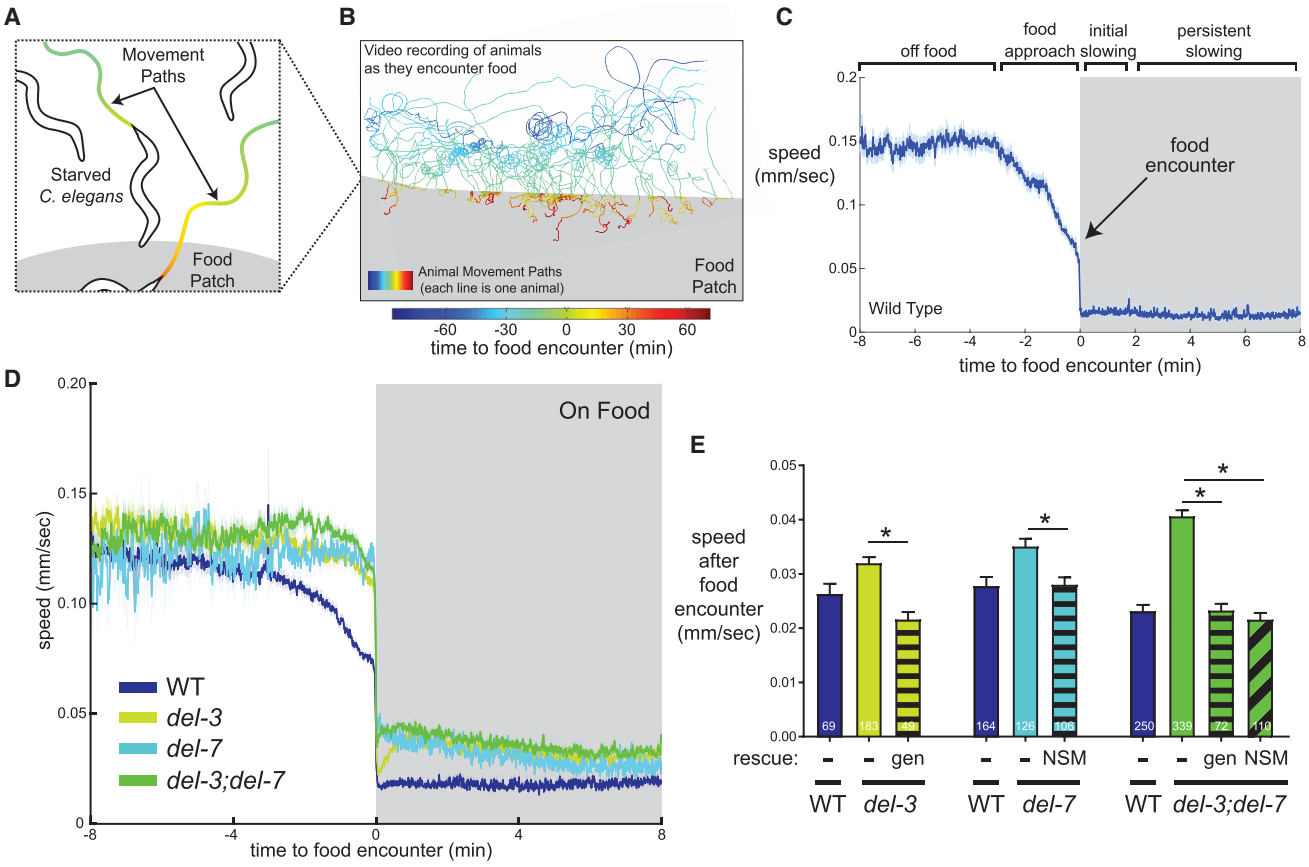

Figure 4. Behavioral Slowing in Response to Food Is Mediated by *del-3* and *del-7* in NSM

(A) Cartoon of animals encountering a bacterial food patch.

(B) Example data from one video with many individual animal movement paths colored by time relative to food encounter.

(C) Average speed of 90 min starved WT animals encountering food, with phases of encounter annotated. Data are from one example dataset (n = 110 animals).

(D) Average speeds of 90min starved WT, *del-3*, *del-7*, and *del-3;del-7* animals encountering food. n ≥ 296 animals in each condition.

(E) Average speed 20–100 s after food encounter for the indicated genotypes. "gen" indicates transgenic expression of *del-3* or *del-7* from genomic fragments; "NSM" indicates transgenic expression of *del-3* or *del-7* cDNAs in NSM. *p < 0.01, ANOVA and Bonferroni-corrected t test. n is indicated in bars.

Data are shown as means ± SEM. See also Figure S4.

NSM calcium peaks that began within seconds of encountering a food patch and lasted ~30 s to 3 min (Figure 5A). NSM activity did not detectably change before animals encountered the food, even as they came into close proximity to the food patch (Figure S5A). Consistent with previous studies, NSM calcium peaks triggered by food encounters were correlated with an abrupt, persistent transition to slow locomotion (Figure 5A, bottom). Across animals, NSM activity was strongly associated with reduced speed immediately after food encounter (Figures 5A and S5B), although the magnitude of NSM activation was not linearly correlated with the magnitude of speed reduction (Figure S5B). Instead, NSM activation appears to trigger an all-or-none transition to slow locomotion, consistent with previous studies (Flavell et al., 2013). This interpretation is also consistent with the observation that optogenetically activating NSM with a range of different light intensities in the presence of food produces the same magnitude of initial slowing when the lights are turned on (Figure S5C).

In contrast to fasted and starved animals, well-fed animals almost never displayed NSM calcium peaks timed to the food patch encounter (Figures 5A–5B). Instead, well-fed animals displayed stochastic, irregular NSM calcium peaks at later time points, as previously described (Flavell et al., 2013). These animals also failed to slow abruptly in response to the food encounter, gradually slowing instead (Figure 5A). These results indicate that NSM's response to food ingestion is modulated by satiety: NSM is immediately activated by food ingestion in starved animals but is inhibited in well-fed animals until its activity is stochastically de-repressed at later time points during feeding.

Satiety states can be communicated through circuit-level mechanisms involving neuropeptide signaling. To examine whether circuit-level mechanisms suppress NSM's sensory response to food in well-fed animals, we measured NSM activity during food patch encounters in well-fed and starved *unc-31* mutants, which are defective in neuropeptide release. There

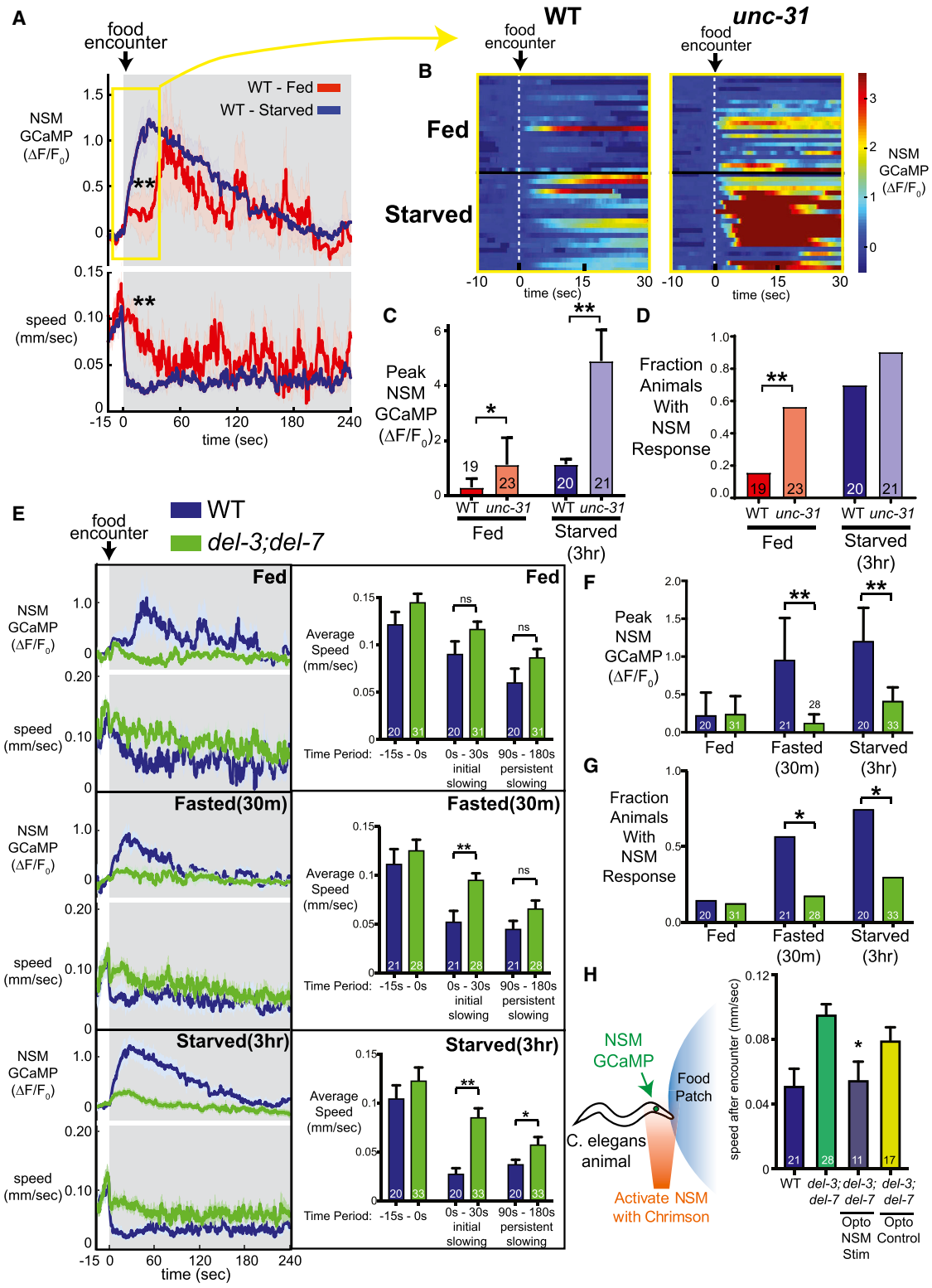

Figure 5. *del-3* and *del-7* Mediate NSM Food Responses Modulated by Satiety State

(A) Average NSM GCaMP and speed of well-fed (red) and 3-hr starved (blue) WT animals encountering food. **p < 0.01, t test.

(B) Heatmaps where each row shows a WT or *unc-31* mutant animal's GCaMP trace over the indicated time frame.

(C) Peak NSM GCaMP signals after food encounters (*p < 0.05 and **p < 0.01, Mann-Whitney test).

(legend continued on next page)

was a robust de-repression of NSM activity in this mutant background in both well-fed and starved animals (Figures 5B–5D). Notably, NSM activation in well-fed *unc-31* animals was as robust as NSM activation in starved WT animals (Figures 5B–5D). These experiments suggest that neuropeptide signaling inhibits NSM activity and that this inhibition is a major component of NSM suppression in well-fed animals.

DEL-3 and DEL-7 Are Required for NSM Calcium Responses to Food, which Drive Slow Locomotion

To examine how DEL-3 and DEL-7 contribute to feeding-dependent NSM activity, we recorded NSM calcium levels in well-fed, fasted, and starved *del-3;del-7* double mutants during food patch encounters. Compared to WT animals, NSM calcium events were abolished in fasted double mutants and greatly attenuated in starved double mutants (Figures 5E–5G). In addition, we observed no stochastic, irregular NSM activity in well-fed double mutants (Figures 5E–5G). Consistent with the above behavioral analyses (Figure 4E), slowing was defective in fasted and starved conditions immediately after food encounter and minutes later, compared to WT (Figures 5E and S5D). Similar defects were also observed in *del-3* and *del-7* single mutants (Figures S5E and S5F). These data indicate that *del-3* and *del-7* are critical for food-induced NSM activity and behavioral slowing.

We asked whether these defects reflect a specific function for DEL-7 and DEL-3 in food detection. To test whether *del-3* and *del-7* play general roles in controlling NSM excitability or calcium influx, we photo-activated NSM with Chrimson in non-feeding animals while recording NSM GCaMP (Figure S5G). We found that activating Chrimson with increasing red light intensities led to stronger NSM GCaMP responses, which decayed after light cessation (Figure S5G). WT and *del-3;del-7* double mutant animals had similar NSM GCaMP responses at all light levels examined (Figure S5G), suggesting these channels do not generically control NSM excitability or calcium influx.

To test whether other DEG/ENaC channels could substitute for *del-3* and *del-7* in mediating NSM food responses, we expressed the known mechanosensor *deg-1* (also in the DEG/ENaC superfamily) in NSM neurons of *del-3;del-7* double mutants, but found this did not restore NSM calcium responses upon food encounter (Figure S5H). Thus, the roles of DEL-3 and DEL-7 in mediating NSM food responses cannot be flexibly substituted by other DEG/ENaC channels.

We hypothesized that the loss of NSM activity in *del-3;del-7* mutants likely causes the deficit in food-induced slowing in this mutant background. To directly test this, we restored WT NSM calcium peaks to *del-3;del-7* mutants at the moment of food encounter and examined the impact on behavior. We again co-expressed Chrimson and GCaMP in NSM in *del-3;del-7* double mutants and then examined the behavior of animals that had been fasted for 30 min. At the moment these animals encountered the food patch, we activated Chrimson with red light (Figure 5H). We shaped the intensity of the red light so that animals received a temporal pattern of red light whose profile matched the kinetics of a WT NSM calcium response to food. Simultaneous NSM calcium imaging confirmed that this approach induced NSM calcium events with similar amplitudes and kinetics to those seen in fasted WT animals (Figure S5I). Furthermore, these animals displayed a slowing response to the food encounter similar to WT animals (Figure 5H). These results indicate that the novel ASICs *del-3* and *del-7* are required for food-induced NSM activity, which in turn drives behavioral slowing.

A Gain-of-Function Point Mutation in *del-7* Alters NSM Calcium Dynamics and Behavioral Dynamics

The above experiments indicate that *del-3* and *del-7* are critical for food-induced NSM activity and behavioral slowing. However, these experiments did not reveal whether these ASICs play an active role in shaping NSM's dynamical response to food ingestion. We reasoned that additional gain-of-function mutations in DEL-3 or DEL-7 that alter the properties of these channels might provide such insights. To better understand how NSM serves its unique role in gut-brain signaling, we performed unbiased forward genetic screens for mutants with defective 5-HTergic vesicle localization in NSM. Remarkably, from this orthogonal approach we also recovered an allele of *del-7*. The *ola110* allele that we recovered contains a point mutation that causes a methionine-to-threonine substitution in amino acid 76 of DEL-7, which is in a juxtamembrane region in the N-terminal intracellular domain. This region has been implicated previously in channel gating and pore properties in related DEG/ENaCs (Figure 3B) (Tavernarakis et al., 2001). In contrast to WT animals that display punctate clusters of 5-HT vesicles in NSM, *del-7*(*ola110*) animals displayed diffusely distributed 5-HT vesicles (Figure S6A). Based on complementation tests and comparisons to *del-7* null animals (Figure S6A), we determined that the *ola110* mutation acts as a genetic gain-of-function with semi-dominant inheritance and is henceforth referred to as *del-7*(*ola110gf*). These data indicate that alterations in the DEL-7 channel can influence 5-HT release sites in NSM, and that the *del-7*(*ola110gf*) allele acts as a genetic gain-of-function.

We next examined the effect of this M76T mutation on animal behavior. Starved *del-7*(*ola110gf*) mutants displayed normal slowing immediately after food encounter, but their slow locomotion was unusually sustained so that *del-7*(*ola110gf*) animals

(D) Fraction of animals displaying a NSM calcium peak in response to food encounter (**$p < 0.01$, Chi-square test).
(E) Average NSM GCaMP and locomotion speed of WT (blue) and *del-3;del-7* (green) animals in fed, fasted, and starved conditions. Right: average speed of animals over indicated time periods (**$p < 0.001$, *$p < 0.05$; ns, not significant; ANOVA and pairwise comparison).
(F) Peak NSM GCaMP signals after food encounters (**$p < 0.01$, Kruskal-Wallis test and multiple-comparison corrected Mann-Whitney test).
(G) Fraction of animals displaying a NSM calcium peak in response to food encounter (*$p < 0.05$, multiple comparison-corrected Chi-square test).
(H) Left: Cartoon of optogenetic rescue strategy. Right: Average speed during initial slowing after food encounters (first 35 s after encounter) for indicated conditions. Opto NSM Stim refers to NSM::Chrimson stimulated animals. Opto Control refers to genetic controls where no red light was applied. *$p < 0.05$ by ANOVA and Bonferroni-corrected t test for *del-3;del-7* versus *del-3;del-7*;Opto NSM Stim.
n is indicated in bars. Data are shown as means ± SEM, except (C) and (F), which are medians ± 95% confidence interval. See also Figure S5.

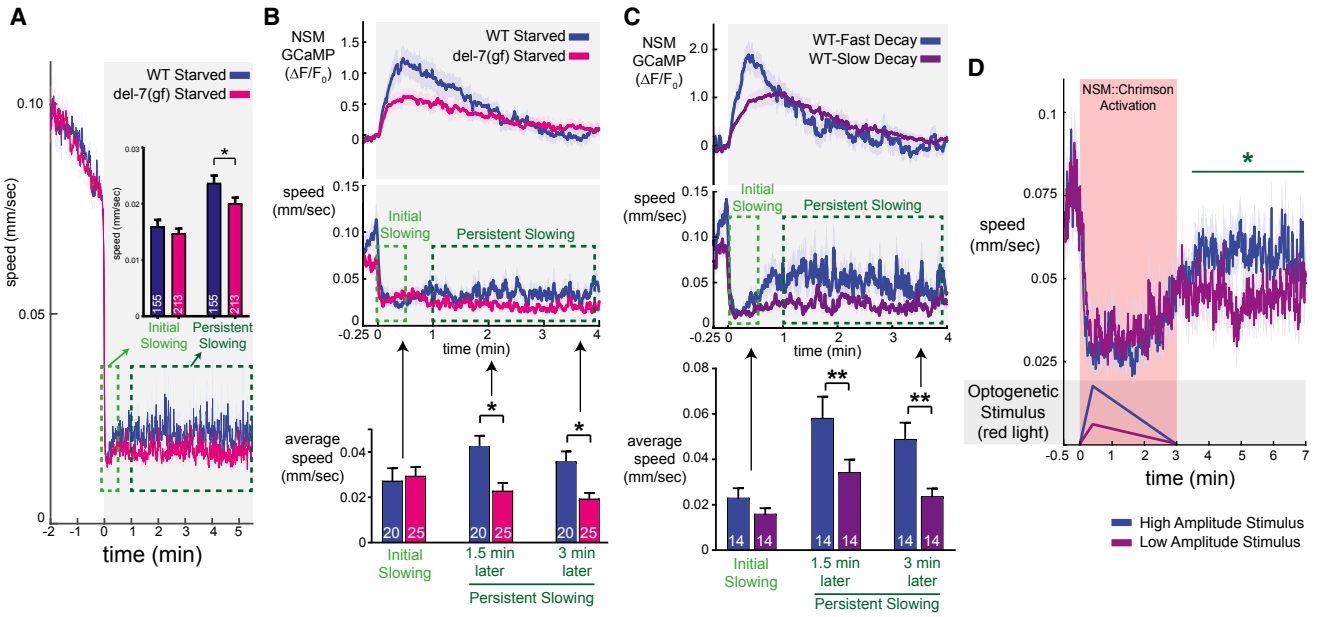

Figure 6. A Point Mutation in DEL-7 Alters NSM Dynamics and Behavioral Dynamics

(A) Average speed surrounding food patch encounters for starved WT and *del-7*(*ola110gf*) animals. Inset: average speed during indicated time periods. *p < 0.05, ANOVA and Bonferroni-corrected pairwise test.

(B) Average NSM GCaMP and speed of WT (blue) and *del-7*(*ola110gf*) (pink) starved animals upon encountering food. *p < 0.05, ANOVA and Bonferroni-corrected pairwise test.

(C) Similar to (B), average NSM GCaMP and locomotion speed for WT animals displaying either high-amplitude, fast-decaying (dark blue), or low-amplitude, slow-decaying (purple) NSM calcium peaks upon food encounters. **p < 0.01, ANOVA and Bonferroni-corrected pairwise test.

(D) Average speed of *del-3;del-7* mutant animals on food in response to high (blue) or low (purple) amplitude optogenetic activation of NSM. Times to peak and decay were identical for these optogenetic stimuli. *p < 0.05, t test. n ≥ 51 animals in each condition.

Data are shown as means ± SEM. n is indicated in bars. See also Figure S6.

had reduced speed relative to WT for many minutes after encountering food (Figure 6A). By comparison, *del-7* null animals had increased speed at all of these time points (Figure 4D). As a genetic control, we induced a frameshift mutation in *del-7*(*ola110gf*) animals that results in a premature stop codon upstream of M76T (Figure S6B). These intragenic revertant *del-7*(*ola110flv3*) animals had a behavioral phenotype matching *del-7* null mutants (Figure S6C), indicating that background mutations in the *del-7*(*ola110gf*) strain are unlikely to explain its defects. These data suggest that *del-7*(*ola110gf*) animals display unusually persistent behavioral slowing in response to food encounter.

We next examined how food-induced NSM calcium dynamics were altered in *del-7*(*ola110gf*) mutants. *del-7*(*ola110gf*) animals displayed an NSM calcium peak of lower amplitude and slower decay rate than that of WT animals (Figure 6B; compare to *del-7*(*lf*) in Figure S6D). Thus, the exaggerated behavioral slowing in response to food encounter in *del-7*(*ola110gf*) is accompanied by a low-amplitude, slow-decaying NSM calcium response upon food encounter, suggesting a potentially complex relationship between NSM calcium events and persistent behavioral slowing.

NSM Dynamics Shape Behavioral Dynamics

Prompted by our observations in the *del-7*(*ola110gf*) mutants, we sought to determine whether different patterns of NSM activity drive different levels of persistent slowing. To examine whether there was a similar relationship between NSM activity and persistent slowing in WT animals as was observed in *del-7*(*ola110gf*) animals, we segmented the WT animals that we had recorded into two groups based on their diverse NSM calcium responses: a low-amplitude/slow-decay group and a high-amplitude/fast-decay group. Like *del-7*(*ola110gf*) mutants, WT animals displaying lower amplitude, slower decaying NSM calcium events displayed lower speed many minutes after food encounter compared with those displaying higher amplitude, faster decaying peaks (Figure 6C; all data points in Figure S6E). Thus, in WT animals NSM calcium dynamics are associated with behavioral dynamics.

To further examine this issue, we optogenetically activated NSM using a variety of stimulation patterns while recording behavior. To avoid interference from endogenous NSM activation, we performed these experiments on *del-3;del-7* mutants. We activated NSM with uniform rise times (24 s to peak, based on endogenous NSM peaks), but varied the decay rate and peak intensity of stimulation. Slower-decaying patterns of NSM stimulation led to more prolonged reductions in locomotion (Figures S6F and S6G). Consistent with our calcium imaging results, we also found that animals receiving low-amplitude optogenetic stimulation displayed a less pronounced rebound in locomotion following light offset compared to animals receiving high-intensity stimulation (Figure 6D). This was most apparent in the time

period immediately after optogenetic stimulation, as both stimuli had similar acute effects on locomotion during the lights-on time period (see also Figures S6F–S6K). Taken together, these data are consistent with the possibility that robust phasic activation of this 5-HTergic neuron drives a transient suppression of locomotion followed by a post-inhibitory rebound, whereas low/moderate increases in NSM activity are more effective at driving persistent slowing.

DISCUSSION

All animals must respond to the ingestion of food by generating adaptive behavioral responses, but the role of gut-brain signaling in behavioral regulation remains poorly understood. Here, we show that the 5-HTergic neuron NSM acts as an enteric sensory neuron that acutely detects food ingestion through a mechanism that requires the newly characterized ASICs, DEL-7 and DEL-3. These channels localize to NSM sensory dendrites in the alimentary canal and are specifically required for responses to food ingestion. Point mutations that alter the DEL-7 channel change NSM dynamics and associated behavioral dynamics. These experiments identify a molecular mechanism for bacterial detection by enteric neurons and illustrate how activity in enteric neurons can drive adaptive behavioral responses to food ingestion.

ASICs Mediate Neuronal Responses to Bacteria and Control Feeding State

Prompted by the finding that NSM acts as an enteric sensory neuron that detects ingested bacteria, we examined the molecular mechanisms that allow this neuron to detect bacterial food cues. Through molecular profiling of NSM, we identified two novel ASICs, DEL-3 and DEL-7, that are required for feeding-dependent NSM activity. We also performed a forward genetic screen that recovered a gain-of-function mutation in *del-7* that enhances the behavioral response to food ingestion. The identification of these ASICs using two orthogonal, unbiased approaches underscores the importance of these channels in NSM. This class of ion channels is highly conserved and mammalian orthologs of *del-3* and *del-7* are expressed in the CNS and in peripheral sensory neurons, such as taste receptor neurons, enteric neurons in the GI system, and dorsal root ganglia nociceptive neurons (Holzer, 2015; Shimada et al., 2006; Wemmie et al., 2013). Given that *del-3* and *del-7* are required in NSM for neural responses to bacteria, we speculate that mammalian orthologs of these channels might mediate responses to bacteria in peripheral sensory neurons, which are also exposed to microbial populations in the mouth, gut, and during bacterial infections.

Our work has not yet fully resolved whether these channels are directly involved in sensory transduction or amplify another primary sensory response in NSM. However, we found that the DEL-7 channels localize to the posterior end of NSM's minor neurite, a dendritic ending that is devoid of synapses, but protrudes into the alimentary canal and is located in close proximity to the site of bacterial lysis in the pharynx. Consistent with a possible sensory function for DEL-7/3 channels in the minor neurite, we found that NSM is acutely and directly activated by bacterial food ingestion and that mutants lacking either the DEL-7/3 channels or the minor neurite had abolished food-induced NSM activity. ASICs can be activated by many agents, including mechanical stimuli and small molecules. For example, DEG/ENaCs are known to mediate touch sensitivity in *C. elegans* sensory neurons (Chalfie, 2009). However, we found that pure mechanical stimuli do not activate NSM. In addition, ASICs were initially identified based on their response to low extracellular pH (Wemmie et al., 2013). However, pharyngeal pH does not change during food ingestion, so this might not be the signal driving NSM activity (Chauhan et al., 2013). Our current results are most consistent with an activation mechanism that involves a heat-insensitive bacterial product, though further studies will be necessary to fully answer this question.

NSM's response to food ingestion is modulated by the animal's satiety state, with well-fed animals showing suppressed and delayed NSM responses to food ingestion, compared to starved animals. We found that mutants defective in neuropeptide release had de-repressed NSM activity. It is possible that this reflects modulation of DEL-3 or DEL-7. ASICs are known to be modulated by neuropeptides, protein kinases, and other intracellular signaling pathways (Wemmie et al., 2013). Indeed, our NSM TRAP studies revealed new NSM-enriched neuropeptide receptors that could merit further investigation across satiety states (Table S1).

Enteric Sensory Neurons Control Behavioral Responses to Food Ingestion

How does patterned activity in the enteric nervous system drive changes in animal behavior? Here, we show that the enteric 5-HTergic neuron NSM integrates its acute detection of food with chronic satiety levels. Depending on the animal's internal state, NSM generates calcium peaks of varying amplitudes and kinetics when it encounters food. NSM calcium peaks uniformly drive acute behavioral slowing, which allows animals to slow down and feed. Our data also suggest the specific pattern of NSM activity shapes long-term locomotion dynamics. High-amplitude, phasic NSM responses drive transient slowing, followed by a rebound speed burst when NSM activity decays. Moderate-amplitude NSM calcium peaks drive both transient and sustained behavioral slowing. However, we note that the relationship between NSM activity and locomotion is complex and that other neurons are likely also involved. The mechanism underlying the rebound speed bursts after phasic NSM activation is still unclear, though it could involve post-inhibitory rebound in downstream neurons, 5-HT receptor desensitization, circuit-level effects, or even co-transmission. Neuromodulation and post-inhibitory rebound are key features of circuits that generate rhythmic oscillations (Marder et al., 2014). Further studies of this circuit may clarify whether similar mechanisms control behavioral state switching. Notably, optogenetic stimulation of 5-HTergic neurons in rodents drives acute behavioral slowing, but repeated stimulation causes increased locomotion afterward (Correia et al., 2017). Thus, 5-HTergic neurons might have a conserved role in driving opposing short- and long-term behaviors.

A previous study found that harmful environmental cues inhibit NSM (Li et al., 2012), which, when combined with our findings, suggests that NSM integrates appetitive (food) and aversive

(harmful) cues. The drive to exploit a food patch is normally balanced by a drive to explore for other food sources. However, indicators of risk or danger in the environment cause animals to favor exploitation over risky exploration. NSM might integrate these disparate cues and generate precisely tuned neural responses that dictate how long to exploit a newly encountered food patch.

Conserved Role for 5-HT in Mediating Gut-to-Brain Signaling

NSM's role as an enteric sensory neuron that signals through 5-HT is reminiscent of 5-HTergic enteroendocrine cells in the mammalian GI epithelium. These cells can detect feeding cues in the gut and release 5-HT that has local and long-range effects (Bellono et al., 2017). 5-HTergic neurons in the mammalian CNS have also been shown to have phasic responses to food ingestion, which can be modulated by internal state (Li et al., 2016). In the compressed nervous system of *C. elegans*, NSM acts as an enteric sensory neuron, an integrator of internal state, and a site of 5-HT release that targets downstream neurons to drive adaptive behavioral responses to food ingestion.

STAR★METHODS

Detailed methods are provided in the online version of this paper and include the following:

- KEY RESOURCES TABLE
- CONTACT FOR REAGENT AND RESOURCE SHARING
- EXPERIMENTAL MODEL AND SUBJECT DETAILS
  - *C. elegans* strains
  - Growth Conditions & Handling
- METHOD DETAILS
  - Forward Genetic Screen and Characterization of del-7(*ola110*gf)
  - Tagged Ribosome Affinity Purification Analysis
  - Reverse Transcription-Quantitative PCR
  - Exploration Behavior Assays
  - Pharyngeal Pumping Assays
  - Food Patch Encounter Behavioral Assays
  - *In vivo* Calcium Imaging
  - Optogenetic Stimulation of NSM During Behavioral Recordings
- QUANTIFICATION AND STATISTICAL ANALYSES
- DATA AND SOFTWARE AVAILABILITY

SUPPLEMENTAL INFORMATION

Supplemental Information includes six figures and one table and can be found with this article online at https://doi.org/10.1016/j.cell.2018.11.023.

ACKNOWLEDGMENTS

We thank Cori Bargmann for support and advice during early phases of this project, Josh Greene for early help with exploration assays, Lucelenie Rodriguez-Laureano for technical help, and David Hall for helpful discussions about NSM morphology. We thank Paul Greer, Cori Bargmann, and members of the Flavell Lab for helpful comments on the manuscript. We thank Olivia Foster Rhoades for her graphical contributions. We also thank the Research Center for Minority Institutions program, the Instituto de Neurobiología de la Universidad de Puerto Rico and the Marine Biological Laboratories for providing a meeting and brainstorming platform. We thank the *Caenorhabditis* Genetics Center (supported by P40 OD010440) for strains. S.W.F. acknowledges funding from the JPB Foundation, PIIF, PNDRF, the NARSAD Young Investigator Award Program, and NIH (R01NS104892). HHMI also supported early phases of this project. D.A.C.-R., and J.C.N. were supported by NIH (R01NS076558), NSF (IOS 1353845), and the Howard Hughes Medical Institute Faculty Scholars program.

AUTHOR CONTRIBUTIONS

J.L.R., J.C.N., I.N., S.K.Y., I.G.M., G.K.M., D.A.C.-R., and S.W.F. designed experiments. J.L.R., J.C.N., I.N., S.K.Y., I.G.M., G.K.M., E.A., J.R.P., and S.W.F. conducted experiments, analyzed data, and interpreted data. J.L.R. and S.W.F. wrote the paper.

DECLARATION OF INTERESTS

The authors declare no competing interests.

Received: February 8, 2018
Revised: August 27, 2018
Accepted: November 14, 2018
Published: December 20, 2018

REFERENCES

Albertson, D.G., and Thomson, J.N. (1976). The pharynx of Caenorhabditis elegans. Philos. Trans. R. Soc. Lond. B Biol. Sci. *275*, 299–325.

Avery, L., Bargmann, C.I., and Horvitz, H.R. (1993). The Caenorhabditis elegans unc-31 gene affects multiple nervous system-controlled functions. Genetics *134*, 455–464.

Axäng, C., Rauthan, M., Hall, D.H., and Pilon, M. (2008). Developmental genetics of the C. elegans pharyngeal neurons NSML and NSMR. BMC Dev. Biol. *8*, 38.

Bellono, N.W., Bayrer, J.R., Leitch, D.B., Castro, J., Zhang, C., O'Donnell, T.A., Brierley, S.M., Ingraham, H.A., and Julius, D. (2017). Enterochromaffin cells are gut chemosensors that couple to sensory neural pathways. Cell *170*, 185–198.

Ben Arous, J., Laffont, S., and Chatenay, D. (2009). Molecular and sensory basis of a food related two-state behavior in C. elegans. PLoS ONE *4*, e7584.

Brenner, S. (1974). The genetics of Caenorhabditis elegans. Genetics *77*, 71–94.

Chalfie, M. (2009). Neurosensory mechanotransduction. Nat. Rev. Mol. Cell Biol. *10*, 44–52.

Chauhan, V.M., Orsi, G., Brown, A., Pritchard, D.I., and Aylott, J.W. (2013). Mapping the pharyngeal and intestinal pH of Caenorhabditis elegans and real-time luminal pH oscillations using extended dynamic range pH-sensitive nanosensors. ACS Nano *7*, 5577–5587.

Choi, S., Chatzigeorgiou, M., Taylor, K.P., Schafer, W.R., and Kaplan, J.M. (2013). Analysis of NPR-1 reveals a circuit mechanism for behavioral quiescence in C. elegans. Neuron *78*, 869–880.

Cohen, J.Y., Amoroso, M.W., and Uchida, N. (2015). Serotonergic neurons signal reward and punishment on multiple timescales. eLife *4*. Published online February 25, 2015. https://doi.org/10.7554/eLife.06346.

Correia, P.A., Lottem, E., Banerjee, D., Machado, A.S., Carey, M.R., and Mainen, Z.F. (2017). Transient inhibition and long-term facilitation of locomotion by phasic optogenetic activation of serotonin neurons. eLife *6*, e20975.

Flavell, S.W., Pokala, N., Macosko, E.Z., Albrecht, D.R., Larsch, J., and Bargmann, C.I. (2013). Serotonin and the neuropeptide PDF initiate and extend opposing behavioral states in C. elegans. Cell *154*, 1023–1035.

Fujiwara, M., Sengupta, P., and McIntire, S.L. (2002). Regulation of body size and behavioral state of C. elegans by sensory perception and the EGL-4 cGMP-dependent protein kinase. Neuron *36*, 1091–1102.

Heiman, M., Schaefer, A., Gong, S., Peterson, J.D., Day, M., Ramsey, K.E., Suárez-Fariñas, M., Schwarz, C., Stephan, D.A., Surmeier, D.J., et al. (2008). A translational profiling approach for the molecular characterization of CNS cell types. Cell *135*, 738–748.

Holzer, P. (2015). Acid-sensing ion channels in gastrointestinal function. Neuropharmacology *94*, 72–79.

Iwanir, S., Brown, A.S., Nagy, S., Najjar, D., Kazakov, A., Lee, K.S., Zaslaver, A., Levine, E., and Biron, D. (2016). Serotonin promotes exploitation in complex environments by accelerating decision-making. BMC Biol. *14*, 9.

Klapoetke, N.C., Murata, Y., Kim, S.S., Pulver, S.R., Birdsey-Benson, A., Cho, Y.K., Morimoto, T.K., Chuong, A.S., Carpenter, E.J., Tian, Z., et al. (2014). Independent optical excitation of distinct neural populations. Nat. Methods *11*, 338–346.

Li, C., and Kim, K. (2008). Neuropeptides. WormBook Online Rev. C. Elegans Biol., 1–36.

Li, Z., Li, Y., Yi, Y., Huang, W., Yang, S., Niu, W., Zhang, L., Xu, Z., Qu, A., Wu, Z., and Xu, T. (2012). Dissecting a central flip-flop circuit that integrates contradictory sensory cues in C. elegans feeding regulation. Nat. Commun. *3*, 776.

Li, Y., Zhong, W., Wang, D., Feng, Q., Liu, Z., Zhou, J., Jia, C., Hu, F., Zeng, J., Guo, Q., et al. (2016). Serotonin neurons in the dorsal raphe nucleus encode reward signals. Nat. Commun. *7*, 10503.

Liu, Z., Zhou, J., Li, Y., Hu, F., Lu, Y., Ma, M., Feng, Q., Zhang, J.-E., Wang, D., Zeng, J., et al. (2014). Dorsal raphe neurons signal reward through 5-HT and glutamate. Neuron *81*, 1360–1374.

Marder, E., O'Leary, T., and Shruti, S. (2014). Neuromodulation of circuits with variable parameters: single neurons and small circuits reveal principles of state-dependent and robust neuromodulation. Annu. Rev. Neurosci. *37*, 329–346.

Mawe, G.M., and Hoffman, J.M. (2013). Serotonin signalling in the gut–functions, dysfunctions and therapeutic targets. Nat. Rev. Gastroenterol. Hepatol. *10*, 473–486.

Nelson, J.C., and Colón-Ramos, D.A. (2013). Serotonergic neurosecretory synapse targeting is controlled by netrin-releasing guidepost neurons in Caenorhabditis elegans. J. Neurosci. *33*, 1366–1376.

Okaty, B.W., Freret, M.E., Rood, B.D., Brust, R.D., Hennessy, M.L., deBairos, D., Kim, J.C., Cook, M.N., and Dymecki, S.M. (2015). Multi-scale molecular deconstruction of the serotonin neuron system. Neuron *88*, 774–791.

Pokala, N., Liu, Q., Gordus, A., and Bargmann, C.I. (2014). Inducible and titratable silencing of Caenorhabditis elegans neurons in vivo with histamine-gated chloride channels. Proc. Natl. Acad. Sci. USA *111*, 2770–2775.

Sanz, E., Yang, L., Su, T., Morris, D.R., McKnight, G.S., and Amieux, P.S. (2009). Cell-type-specific isolation of ribosome-associated mRNA from complex tissues. Proc. Natl. Acad. Sci. USA *106*, 13939–13944.

Saper, C.B., Fuller, P.M., Pedersen, N.P., Lu, J., and Scammell, T.E. (2010). Sleep state switching. Neuron *68*, 1023–1042.

Sawin, E.R., Ranganathan, R., and Horvitz, H.R. (2000). C. elegans locomotory rate is modulated by the environment through a dopaminergic pathway and by experience through a serotonergic pathway. Neuron *26*, 619–631.

Shimada, S., Ueda, T., Ishida, Y., Yamamoto, T., and Ugawa, S. (2006). Acid-sensing ion channels in taste buds. Arch. Histol. Cytol. *69*, 227–231.

Tavernarakis, N., Everett, J.K., Kyrpides, N.C., and Driscoll, M. (2001). Structural and functional features of the intracellular amino terminus of DEG/ENaC ion channels. Curr. Biol. *11*, R205–R208.

Waggoner, L.E., Zhou, G.T., Schafer, R.W., and Schafer, W.R. (1998). Control of alternative behavioral states by serotonin in Caenorhabditis elegans. Neuron *21*, 203–214.

Wemmie, J.A., Taugher, R.J., and Kreple, C.J. (2013). Acid-sensing ion channels in pain and disease. Nat. Rev. Neurosci. *14*, 461–471.

STAR★METHODS

KEY RESOURCES TABLE

REAGENT or RESOURCE	SOURCE	IDENTIFIER
Antibodies		
Mouse monoclonal anti-HA	Sigma-Aldrich	Cat#H3663; RRID: AB_262051
Bacterial and Virus Strains		
E. coli: Strain OP50	*Caenorhabditis* Genetics Center	OP50
Chemicals, Peptides, and Recombinant Proteins		
Nuclease-free magnesium chloride	ThermoFisher	Cat#9530G
Nuclease-free potassium chloride	ThermoFisher	Cat#9640G
Nuclease-free water	ThermoFisher	Cat#AM9939
1,2,-dihetpanoyl-sn-glycero-3-phosphocholine (DHPC)	Avanti Polar Lipids	Cat#850306P
Recombinant RNasin	Promega	Cat#N2515
Complete, Mini, EDTA-free protease inhibitor cocktail	Roche	Cat#4693124
DL-Dithiothreitol (DTT)	Sigma-Aldrich	Cat#D9779
Cycloheximide	Sigma-Aldrich	Cat#C7698
NP-40	Sigma-Aldrich	Cat#I8896
Tetramethyl sulfolane	Sigma-Aldrich	Cat#T2209
Ribonucleoside vanadyl complex	New England Biolabs	Cat#S1402S
Protein G Dynabeads	Life Technologies	Cat#10004D
HEPES, pH 7.3	Alfa Aesar	Cat#J16924-AE
All-trans-retinal	Sigma-Aldrich	Cat#R2500
Histamine dihydrochloride	Sigma-Aldrich	Cat#H7250
Phenol Red	Sigma-Aldrich	Cat#P3532
Critical Commercial Assays		
Absolutely RNA Nanoprep Kit	Agilent	Cat#400753
Ovation RNA amplification system v2	NuGEN	Cat#3100-12
Clontech SMARTer Ultra Low Input RNA	Clontech	Cat#634820
Nextera XT Library Prep Kit	Illumina	Cat#FC-131-1096
Deposited Data		
Raw and analyzed data	This paper	GEO: GSE110334
Experimental Models: Organisms/Strains		
C. elegans: Wild-type Bristol N2	*Caenorhabditis* Genetics Center	N2
C. elegans: *del-7(ok1187)*	This paper	SWF17
C. elegans: *del-3(ok2613)*	This paper	CX16813
C. elegans: *del-7(ok1187);del-3(ok2613)*	This paper	SWF18
C. elegans: *del-7(ola110)*	This paper	SWF86
C. elegans: *del-7(ola110flv3)*	This paper	SWF145
C. elegans: *del-7(gk688559)*	This paper	CX16404
C. elegans: *flvEx30[Ptph-1::GCaMP5a, Ptph-1::mCherry, Psrg-47::GCaMP5a, Psrg-47::mCherry]*	This paper	SWF62
C. elegans: *del-7(ok1187); flvEx31[Pdel-7::del-7-sl2-GFP, myo-3::mCherry]*	This paper	SWF63
C. elegans: *del-3(ok2613); flvEx32[del-3- genomic-sl2-GFP, myo-3::mCherry]*	This paper	SWF64
C. elegans: *del-7(ok1187); del-3(ok2613); flvEx30[Ptph-1::GCaMP5a, Ptph-1::mCherry, Psrg-47::GCaMP5a, Psrg-47::mCherry]*	This paper	SWF65

(*Continued on next page*)

Continued

REAGENT or RESOURCE	SOURCE	IDENTIFIER
C. elegans: *del-7(ok1187); del-3(ok2613); flvEx33[del-7- genomic-sl2-GFP, del-3- genomic-sl2- GFP, myo-3::mCherry]*	This paper	SWF68
C. elegans: *unc-101(m1) I; flvEx30[Ptph-1::GCaMP5a, Ptph-1::mCherry, Psrg-47::GCaMP5a, Psrg-47::mCherry]*	This paper	SWF84
C. elegans: *del-7(ok1187); del-3(ok2613); flvEx30[Ptph-1::GCaMP5a, Ptph-1::mCherry, Psrg-47::GCaMP5a, Psrg-47::mCherry]; kyEx5717 [tph-1(short)::Chrimson, elt-2::mCherry]*	This paper	SWF89
C. elegans: *del-7(ola110); flvEx30[Ptph-1::GCaMP5a, Ptph-1::mCherry, Psrg-47::GCaMP5a, Psrg-47::mCherry]*	This paper	SWF94
C. elegans: *del-7(ok1187); del-3(ok2613); flvEx50[Ptph-1(short)::del-7-sl2- GFP, Ptph-1(short)::del-3-sl2- GFP, myo-3::mCherry]*	This paper	SWF97
C. elegans: *del-7(ok1187); del-3(ok2613); flvEx30[Ptph-1::GCaMP5a, Ptph-1::mCherry, Psrg-47::GCaMP5a, Psrg-47::mCherry]; kyEx5717 [tph-1(short)::Chrimson, elt-2::mCherry]*	This paper	SWF99
C. elegans: *del-7(ok1187);del-3(ok2613); flvEx73[tph-1(short)::GFP PCR product, myo-3::mCherry]*	This paper	SWF139
C. elegans: *unc-13(s69); lite-1(ce314); kyEx4656 [tph-1-NSM-fragment::GCaMP5A; myo-3::mCherry]*	This paper	CX15485
C. elegans: *unc-31(e928); lite-1(ce314); kyEx4656*	This paper	CX15613
C. elegans: *unc-13(s69); lite-1(ce314); aex-6(sa24); kyEx4656*	This paper	CX16188
C. elegans: *unc-13(s69); lite-1(ce314); kyEx5170 [rig-3::GCaMP5A]*	This paper	CX16613
C. elegans: *unc-13(s69); lite-1(ce314); kyIs689 [myo-2::Chrimson; elt-2::his4.4-mCherry]; kyEx4656*	This paper	CX16579
C. elegans: *kyIs694 [tph-1-NSM-fragment::rpl-22-3xHA; tph-1-NSM-fragment::GFP]*	This paper	CX16651
C. elegans: *unc-31(e928) IV; flvEx30[Ptph-1::GCaMP5a, Ptph-1::mCherry, Psrg-47::GCaMP5a, Psrg-47::mCherry]*	This paper	SWF127
C. elegans: *del-7(ok1187); flvEx30[Ptph-1::GCaMP5a, Ptph-1::mCherry, Psrg-47::GCaMP5a, Psrg-47::mCherry]*	This paper	SWF66
C. elegans: *del-3(ok2613); flvEx30[Ptph-1::GCaMP5a, Ptph-1::mCherry, Psrg-47::GCaMP5a, Psrg-47::mCherry]*	This paper	SWF67
C. elegans: *del-7(ok1187); del-3(ok2613); flvEx66[Ptph-1(short)::deg-1, Pelt-2::mCherry]; flvEx30[Ptph-1::GCaMP5a, Ptph-1::mCherry, Psrg-47::GCaMP5a, Psrg-47::mCherry]*	This paper	SWF128
C. elegans: *unc-13(s69) I; flvEx30[Ptph-1::GCaMP5a, Ptph-1::mCherry, Psrg-47::GCaMP5a, Psrg-47::mCherry]*	This paper	SWF134
C. elegans: *flvIs2[tph-1(short)::Chrimson, elt-2::mCherry]; flvEx30 [Ptph-1::GCaMP5a, Ptph-1::mCherry, Psrg-47::GCaMP5a, Psrg-47::mCherry]*	This paper	SWF123
C. elegans: *del-7(ok1187); del-3(ok2613); flvIs2[tph-1(short)::Chrimson, elt-2::mCherry]; flvEx30[Ptph-1::GCaMP5a, Ptph-1::mCherry, Psrg-47::GCaMP5a, Psrg-47::mCherry]*	This paper	SWF126
C. elegans: *twk-10(ky1026)*	This paper	CX1026
C. elegans: *R11F4.2(ky1025)*	This paper	CX1025
C. elegans: *glc-3(ok321)*	*Caenorhabditis* Genetics Center	RB594
C. elegans: *srt-30(gk397985)*	This paper	SWF14
C. elegans: *lgc-47(ok2963)*	*Caenorhabditis* Genetics Center	RB2187
C. elegans: *npr-32(ok2541)*	This paper	CX16812
C. elegans: *kvs-3(nf140)*	*Caenorhabditis* Genetics Center	LY140
C. elegans: *del-7(gk688559); olaIs1*	This paper	DCR2050
C. elegans: *del-7(ola110); olaIs1*	This paper	DCR4685
C. elegans: *del-7(flv6)*	This paper	SWF163

(*Continued on next page*)

Continued		
REAGENT or RESOURCE	SOURCE	IDENTIFIER
C. elegans: *del-7(flv6); unc-119(ox819); flvEx82[tph-1:: myristoylated-mNeptune]*	This paper	SWF164
C. elegans: *kyEx5178[tph-1(short)::HisCl1-sl2-mCherry]*	This paper	CX15388
C. elegans: *olaEx388[Pdel-7::UtrCH::GFP]*	This paper	DCR649
Recombinant DNA		
pJLR11 [*tph-1(short NSM fragment)::del-7-sl2-GFP*]	This paper	N/A
pJLR12 [*tph-1(short NSM fragment)::del-3-sl2-GFP*]	This paper	N/A
pSF214 [*tph-1(short NSM fragment)::rpl-22-3xHA*]	This paper	N/A
Software and Algorithms		
MATLAB (R2017b)	Mathworks	https://www.mathworks.com
ImageJ (v1.50)	NIH	https://imagej.nih.gov/ij/
Fiji (v1.52)	NIH	http://fiji.sc/
Prism (v7.03)	Graphpad	https://www.graphpad.com
NIS-Elements (v4.51.01)	Nikon	https://www.nikoninstruments.com/products/software
Streampix (v7.0)	Norpix	https://www.norpix.com
Other		
Orca Flash 4.0 sCMOS camera	Hamamatsu	N/A
Zyla 4.2 Plus sCMOS camera	Andor	N/A
X-Cite 120LED System XT120L	Lumen Dynamics	N/A
SOLA-LE LED system	Lumencor	N/A
Ti-S Inverted Microscope	Nikon	N/A
SP-20000M-USB3 CMOS camera	JAI	N/A
Micro-NIKKOR 55mm f/2.8 lens	Nikon	N/A
10x25 White Panel LED backlight, 24VDC	Metaphase Technologies	Cat#MS-BL10X25-W-24-ILD-PS
Precision LED Spot Light, 625nm, 40W, Type H	Mightex	Cat#BLS-PLS-0625-030-40-S
BioLED Light Source Control Module	Mightex	Cat#BLS-13000-1

CONTACT FOR REAGENT AND RESOURCE SHARING

Further information and requests for resources and reagents should be directed to and will be fulfilled by Lead Contact, Steven W. Flavell (flavell@mit.edu).

EXPERIMENTAL MODEL AND SUBJECT DETAILS

C. elegans strains

All wild-type, mutant and transgenic strains used in this study are listed in the Key Resources Table above.

Growth Conditions & Handling

Nematode culture was conducted using standard methods (Brenner, 1974). Populations were maintained on NGM agar plates supplemented with *E. coli* OP50 bacteria. Wild-type was *C. elegans* Bristol strain N2. For genetic crosses, all genotypes were confirmed using PCR. Transgenic animals were generated by injecting DNA clones plus fluorescent co-injection marker into gonads of young adult hermaphrodites. We typically analyzed 2-3 independent transgenic lines per injection. One day old isogenic hermaphrodites were used for all assays. All assays were conducted at room temperature (~22°C) and replicated on two or more days.

METHOD DETAILS

Forward Genetic Screen and Characterization of del-7(*ola110*gf)

The *ola110* mutant was recovered in a forward genetic screen for mutants with altered NSM 5-HT release sites (Nelson and Colón-Ramos, 2013). These mutants displayed a diffuse pattern of the CAT-1::GFP vesicle marker, although active zone markers were

normally localized in NSM. We initially mapped *ola110* to the right arm of Chromosome IV through chromosome mapping. Subsequent interval mapping placed the *ola110* lesion within a 0.55 centiMorgan interval (between SNPs haw57407 and haw153809). Genomic DNA was then collected from *ola110* mutants and sent for whole genome sequencing. Within the region of interest, only 2 non-synonymous mutations were identified. These lesions, subsequently confirmed by Sanger sequencing, included a missense lesion in the gene *K07H8.5*, and a missense lesion in the predicted degenerin/epithelial Sodium channel (DEG/ENaC), *del-7* (M76T). The allele is a presumed gain-of-function because none of the *ola110* mutant phenotypes are observed in the *del-7* null animals, but the phenotype can be reverted to a null phenotype via introduction of a frameshift mutation that induces a premature stop codon upstream of the M76T mutation in *del-7*. This mutation was introduced via CRIPSR/Cas9 using the Co-CRISPR method and is a 17-bp insertion that causes a premature stop codon. The sequence of the modified allele proximal to this mutation is gcttccgtaaacacaacacaTGACACAATATGACACAatatgaggaagctttgaaaa (insertion in capital letters; premature stop codon underlined).

Tagged Ribosome Affinity Purification Analysis

Raw RNA-seq data and processed data analysis files for tagged ribosome affinity purification (TRAP) experiments are freely available in NCBI GEO Datasets (GEO: GSE110334).

We adapted the TRAP method for use in single *C. elegans* neurons, guided by previous protocols used in mammalian tissues (Heiman et al., 2008; Sanz et al., 2009). A Ribotag plasmid was constructed by fusing the *C. elegans rpl-22* (*C27A2.2a*) cDNA with three tandem HA tags (rpl-22-3xHA). Plasmid design was based on the mammalian Ribotag (Sanz et al., 2009). A transgenic strain was generated that expressed both the Ribotag and GFP specifically in NSM. For each TRAP experiment, animals were synchronized by bleaching and grown on 15cm, OP50-seeded NGM plates with enriched peptone (20 g/L). After three days, one-day old adult animals were prepared for lysis by collecting animals from the plates in liquid NGM supplemented with cycloheximide (CHX; 0.8 mg/ml). Animals were washed once in NGM+CHX, and then washed once in Minimal Homogenization Buffer (10mM HEPES, pH 7.4, 150mM KCl, 5mM MgCl2, 0.8 mg/ml CHX). Finally, the worm pellet was resuspended in Complete Homogenization Buffer (10mM HEPES, pH 7.4, 150mM KCl, 5mM MgCl2, 0.5mM DTT, Complete EDTA-free protease inhibitor, 0.4U/uL RNasin, 10mM ribonucleoside vanadyl complex, 0.8 mg/ml CHX). The resuspended animals were flash frozen in liquid nitrogen and stored at −80C.

The concentration of animals was estimated by counting the number of animals in 10uL of frozen solution. Then, frozen worm pellets were ground to a fine powder with an RNase-free pestle while keeping samples frozen. For immunoprecipitations, the samples were thawed, diluted in Complete Homogenization Buffer (as above, except with CHX at 0.1 mg/ml) to a final concentration of 8 animals per uL of extract. Based on the total volume of extract used in each TRAP experiment, we estimate that each pulldown was from ~150,000 animals. NP-40 (1% final) and DHPC (30mM final) detergents were added to the diluted samples. After 10min of 4°C incubation, samples were cleared twice by spinning at 15,000r*cf.* for 12min at 4°C. Samples were then pre-cleared by incubating 150uL Protein G Dynabeads (Life Technologies) with samples for 30' and then discarding the beads. After pre-clearing, 3.5 uL of anti-HA antibody (clone HA-7, Sigma) was incubated with sample for 30min, after which 150uL of Protein G Dynabeads were added and the sample was incubated for an additional 30min. The beads were then washed four times in Wash Buffer (10mM HEPES, pH 7.4, 350mM KCl, 5 mM MgCl2, 1% NP-40, 0.5mM DTT, 0.04U/uL RNasin, 0.1mg/mL CHX). Finally, RNA was eluted from beads by incubating with 100uL of Lysis Buffer from the Absolutely RNA Nanoprep kit (Stratagene). RNA was then purified, following the kit protocol. For whole-animal input material, RNA was also purified from 100uL of the pre-cleared lysate.

Whole-animal and NSM-Ribotag RNA samples were subject to mRNA-seq. We performed three independent biological replicates, as described in the main text. Due to low RNA amounts, samples were first amplified with Clontech SMARTer Ultra Low RNA kit and then prepared for sequencing with Illumina Nextera XT. We obtained 13-93M mapped reads per sample and used CuffLinks to identify genes with increased abundance in NSM-Ribotag samples. For the data shown in Figure 2 and Table S1, we required that each "NSM-enriched" gene (1) was 4-fold enriched in the NSM-Ribotag sample (versus whole-animal) in all three biological replicates, (2) was < 4-fold enriched in a mRNA-seq Ribotag pulldown from a different neuron, and (3) had FPKM values > 0.25 in all three biological replicates.

Reverse Transcription-Quantitative PCR

A subset of genes was tested to validate whether or not they were enriched in NSM Ribotag samples. Each gene's expression was measured using reverse transcription-quantitative PCR (RT-qPCR). cDNA samples were prepared using Nugen Ovation RNA amplification system v2. Expression of specific mRNAs were measured in NSM-Ribotag and Whole-animal RNA samples by qPCR. In these experiments, we used Power SYBR Master Mix and a QuantStudio Realtime PCR system (Life Technologies). For each primer set, we performed standard curves to ensure that amplification was exponential, and a no-reverse-transcriptase control to ensure that there was no genomic DNA contamination. Primer sequences are available upon request.

Exploration Behavior Assays

Behavioral assays for exploration were conducted as previously described (Flavell et al., 2013). L4 animals were picked to 35mm plates seeded with OP50. After 16 hours, plates were superimposed on a grid and the number of squares intersected by the animal's movement path were counted. This assay essentially measures the level of exploration of each animal, which correlates with the level of roaming across many genotypes (Flavell et al., 2013). Data were always normalized to N2 controls measured in parallel.

Pharyngeal Pumping Assays

Pharyngeal pumping was either counted manually (for *myo-2::Chrimson* line) or by video recording and subsequent manual counting (for WT, *del-7;del-3* and *unc-101*). Videos were recorded at 20Hz for 30sec on a tracking microscope stage that followed each freely-moving animal for 30sec on or off food, as indicated in figures. Pharyngeal pumps were counted over this time frame on videos played back in slow motion.

Food Patch Encounter Behavioral Assays

In an assay adapted from Iwanir et al. (2016), wild-type, transgenic, and mutant one-day old adult worms were allowed to re-encounter lawns of OP50 after various levels of starvation. 16 hours prior to assays, 114x73mm NGM plates were seeded with OP50 to create a lawn with a straight edge that covered approximately 2/3 of the plate from edge to edge. For pH measurements, plates were made similarly, but Phenol Red (Sigma) was added at 18mg/L. Prior to assays, one-day old adult worms were washed off standard growth plates with 1 mL of M9 buffer and transferred to 1.7mL Eppendorf tubes, where they were rinsed once with 1mL of M9 before being transferred either to unseeded NGM plates for starvation, or directly to assay plates. For HisCl1 experiments, histamine dihydrochloride (Sigma) was added at 10mM to both the pre-starvation plates and to assay plates. Animals starved before assays were left on unseeded plates for indicated durations of time before transfer to assay plates in M9.

Animals were recorded at 3 fps using Streampix 7.0, a JAI SP-20000M-USB3 CMOS camera (41mm, 5120x3840, Mono) and a Nikon Micro-NIKKOR 55mm f/2.8 lens. Backlighting was achieved using a white panel LED (Metaphase Technologies Inc. White Metastandard 10'' X 25,'' 24VDC). Assay plates were placed on glass 3'' above LEDs to avoid heat transfer to plates. Videos were processed using custom MATLAB scripts, which included a step to manually confirm the exact frame of lawn encounter for each animal.

For experiments with *myo-2::Chrimson* inhibition of pumping (Figure S4C), animals were grown on 50uM all-trans-retinal overnight, and red light was applied constantly during recordings using a 625nm Mightex BioLED light source.

We have plotted the absolute speed of animals throughout all datasets in an effort to present the maximum amount of information with regards to animal behavior, but also present speed data normalized to pre-food-encounter baselines in Figures S4 and S5.

Throughout the study, genetic mutants are compared to complete datasets of wild-type N2 animals.

In vivo Calcium Imaging

In vivo calcium imaging of NSM was conducted in wild-type, transgenic, and mutant backgrounds. For calcium imaging in *unc-13* and *unc-31* mutant backgrounds, experiments were conducted with a 5x/0.25NA Zeiss objective and a Hamamatsu Orca Flash 4.0 sCMOS camera, or a 4x/0.2NA Nikon objective and an Andor Zyla 4.2 Plus sCMOS camera. Blue light application to animals was 10ms for each exposure at a rate of 10fps, as previously described (Flavell et al., 2013). In these experiments, one-day old adult animals were picked to flat NGM pads that either had (i) no bacteria, (ii) OP50, (iii) Aztreonam-treated OP50 (Ben Arous et al., 2009), (iv) heat-killed bacterial extract (95°C for 10min, with vortexing), (v) heat-killed bacterial extract supernatant (95°C for 10min; then 2 consecutive 15min spins at 17,000xg), or (vi) bacterial-sized beads (Fluorspheres with bead sizes 0.02um-1um in equal parts, Invitrogen) dialyzed into pH5 solution, with 5mM 5-HT to promote bead ingestion. The NGM pads were enclosed using a rubber gasket and cover glass. Animals were imaged for 30 minutes, beginning 15 minutes after they were transferred. Pixel intensity values for NSM and adjacent background were extracted from each video frame using custom ImageJ macros, as described previously (Flavell et al., 2013). Gaps in recordings were due to animals adopting a body posture that obscured the head. For these recordings where animals were chronically on or off food, background-subtracted NSM GCaMP fluorescence values were normalized to baseline periods of NSM inactivity for each trace. For experiments with combined *myo-2::Chrimson* inhibition of pumping, animals were grown on 1-3uM all-trans-retinal overnight, and blue light levels were reduced to 1%–5% output on the SOLA-LE solid-state LED light source. Red light was applied at defined times using a 617nm red LED light (Mightex). Under these recording conditions, blue light did not visibly alter pharyngeal pumping, but red light exposure caused a full cessation of pumping.

The above procedure was adapted to allow for imaging of one-day old adult animals during lawn encounters. Experiments were conducted with a 4x/0.2NA Nikon objective and an Andor Zyla 4.2 Plus sCMOS camera. Blue light application to animals was 100% output from a X-Cite 120LED system for 10ms of each exposure at a recording rate of 10fps, as above. Fed animals, as well as animals fasted for 30 minutes or starved for 3 hours were assayed on flat NGM pads enclosed by a rubber gasket and coverslip as described above. Pads were seeded with 20x concentrated OP50 liquid culture, and rectangular corrals laser cut from Apollo Laser Printer Transparency Film were placed on the slides to keep animals within the field of view while recording their food encounter. For experiments with combined Chrimson activation of NSM, animals were grown on 1-3uM all-trans-retinal overnight, and blue light levels were reduced to two 2-ms pulses 6ms apart at 20% intensity. For Optogenetic Rescue experiments, recordings were monitored so that red light application (617nm Mightex LED) was timed with each animal's food encounter. For activation of NSM in non-feeding animals, red light was applied for 30sec at intensities indicated in figure to animals immobilized in tetramisole. Under these recording conditions, blue light did not visibly alter NSM activation on or off food.

Optogenetic Stimulation of NSM During Behavioral Recordings

For optogenetic stimulation of NSM during behavioral recordings, L4 animals were picked onto 50uM all-trans-retinal (ATR) OP50 plates 16-24 hours before experiments. Where indicated, control animals were cultivated on plates without ATR.

15cm NGM plates used for 'on food' experiments were seeded evenly with 600ul of OP50 and let dry overnight. Immediately prior to experiments, a thin filter paper ring 1-1.5 cm wide, with a 15cm outer diameter, was dipped in 0.02M copper chloride solution and placed on either unseeded 15cm NGM plates ('off food') or seeded NGM plates ('on food'). *C. elegans'* aversion to heavy metals makes these copper rings useful in preventing animals from leaving the recording arena.

For behavioral recordings, one-day old adult animals were picked directly from ATR or control plates to the copper ringed 'on food' plates 45 minutes before experiments. In 'off food' experiments, animals were washed twice with liquid NGM solution to remove all bacteria, then placed on copper ringed NGM plates 15 minutes before experiments.

Animals were illuminated with 625nm red light from a Mightex BioLED while being recorded via the Streampix setup described above. Illumination patterns were delivered to the BioLED Light Source Control Module via custom MATLAB scripts.

QUANTIFICATION AND STATISTICAL ANALYSES

The statistical tests performed in this study are indicated in the figure legends and Results section.

DATA AND SOFTWARE AVAILABILITY

The accession number for the NSM TRAP mRNA-Seq datasets, including raw and processed data files, reported in this paper is GEO: GSE110334.

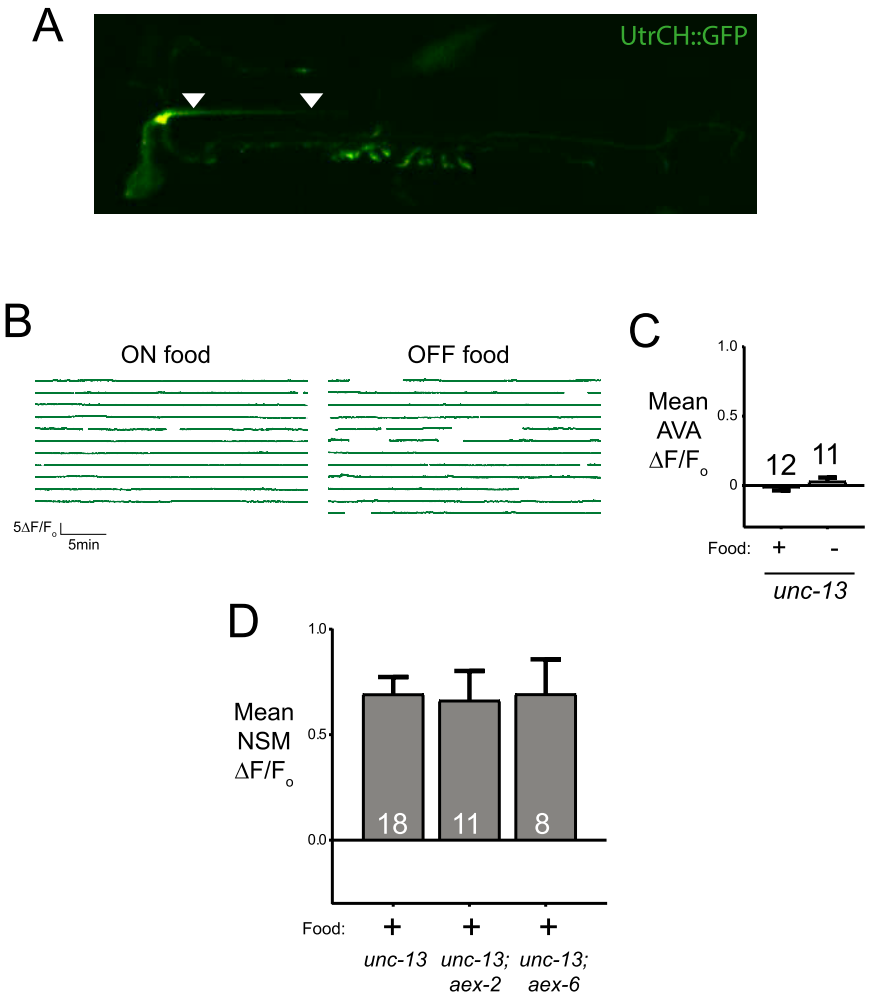

Figure S1. Controls Related to Feeding-Dependent NSM Activity, Related to Figure 1

(A) Enrichment of F-actin in the minor neurite of NSM. In this representative image, NSM expresses the calponin homology domain of utrophin fused to GFP (UtrCH::GFP), which localizes to the NSM minor neurite, indicated by arrowheads. (B) GCaMP imaging of AVA neurons in *unc-13(s69)* mutants, in the presence or absence of food. Data are shown as in Figure 1B. Note that AVA does not show spontaneous activity while feeding and does not display differences in presence versus absence of food. Thus, the NSM activity patterns observed in this context are not broadly observed across neurons. (C) Average AVA GCaMP signals, presented as in Figure 1C. n is indicated over bars. (D) *aex-2* and *aex-6* do not affect NSM calcium signals. Average NSM GCaMP signals in *unc-13(s69)* mutant background with additional mutations in *aex-2* or *aex-6*. These mutations alter intestine-to-brain signaling via a disruption in intestinal peptide release (by AEX-6, a Rab GTPase) or loss of a GPCR (AEX-2) that responds to intestinal neuropeptides. n is indicated in bars. For C-D, data shown as means ± SEM.

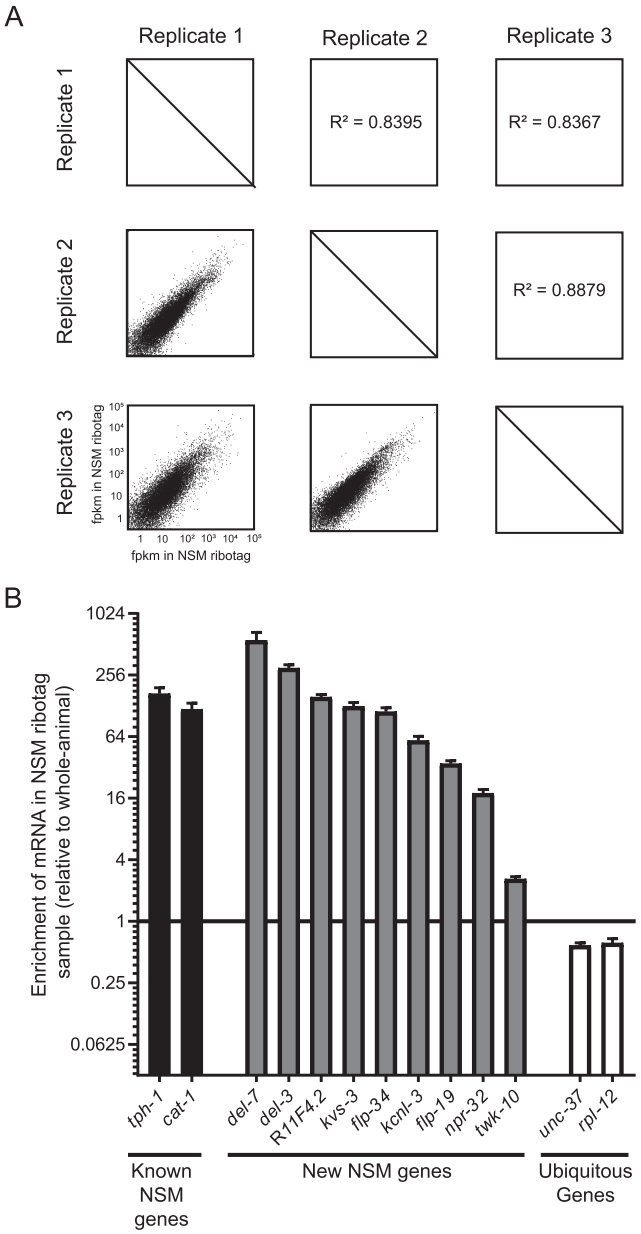

Figure S2. Analyses Related to NSM TRAP, Related to Figure 2

(A) NSM TRAP biological replicates show similar results. Scatterplots in lower left show pairwise comparisons between biological replicates, where each gene's fpkm value in the NSM TRAP sample is shown in each replicate. Correlation coefficients corresponding to these plots are shown in the upper right. (B) Single gene validation of mRNA-seq results for the NSM TRAP experiments. These data are from quantitative reverse transcription-PCR (qRT-PCR) measurements of the indicated mRNAs using specific primers for each mRNA. Each mRNA was measured across multiple TRAP replicates (both NSM IP and whole-animal Input) and was normalized to the ubiquitously expressed *cdc-42* mRNA, which closely matched other ubiquitous genes like *unc-37* and *rpl-12*. Here, we display the normalized values in the NSM IP sample, relative to whole-animal mRNA. With the exception of *twk-10*, we were able to validate all genes that were examined, including *del-3* and *del-7*. Data are shown as means ± SEM.

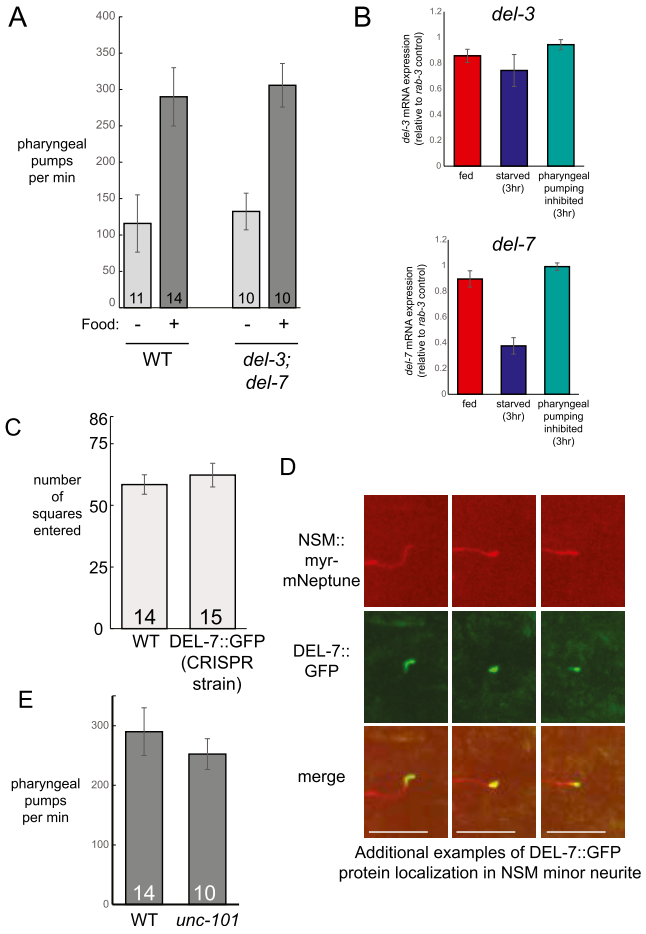

Figure S3. Further Characterization of the Novel DEL-3 and DEL-7 Ion Channels, Related to Figure 3

(A) Pharyngeal pumping rates of WT and *del-3;del-7* mutant animals in the absence or presence of food, displayed as means ± standard deviation. n is indicated in bars. (B) RT-qPCR for *del-3* and *del-7* in animals that were well-fed, starved for 3hrs, or prevented from eating food by inhibiting pharyngeal muscle contraction optogenetically for 3hrs. Expression of each gene was normalized to *rab-3* as a general neuronal marker gene. Data are shown as means ± SEM (C) Exploration assays for WT and *del-7::GFP* animals show no difference between the two strains. Thus, the addition of a C-terminal GFP to native DEL-7 does not result in the *del-7* loss-of-function phenotype shown in Figure 2E. n is indicated in bars. (D) Additional example images of DEL-7::GFP channel subcellular localization in the posterior end of the NSM minor neurite. Images are displayed like the detail in Figure 3G. All scale bars are 10 μm. (E) Pharyngeal pumping rates in WT and *unc-101* mutant animals with data shown as means ± standard deviation. n is indicated in bars.

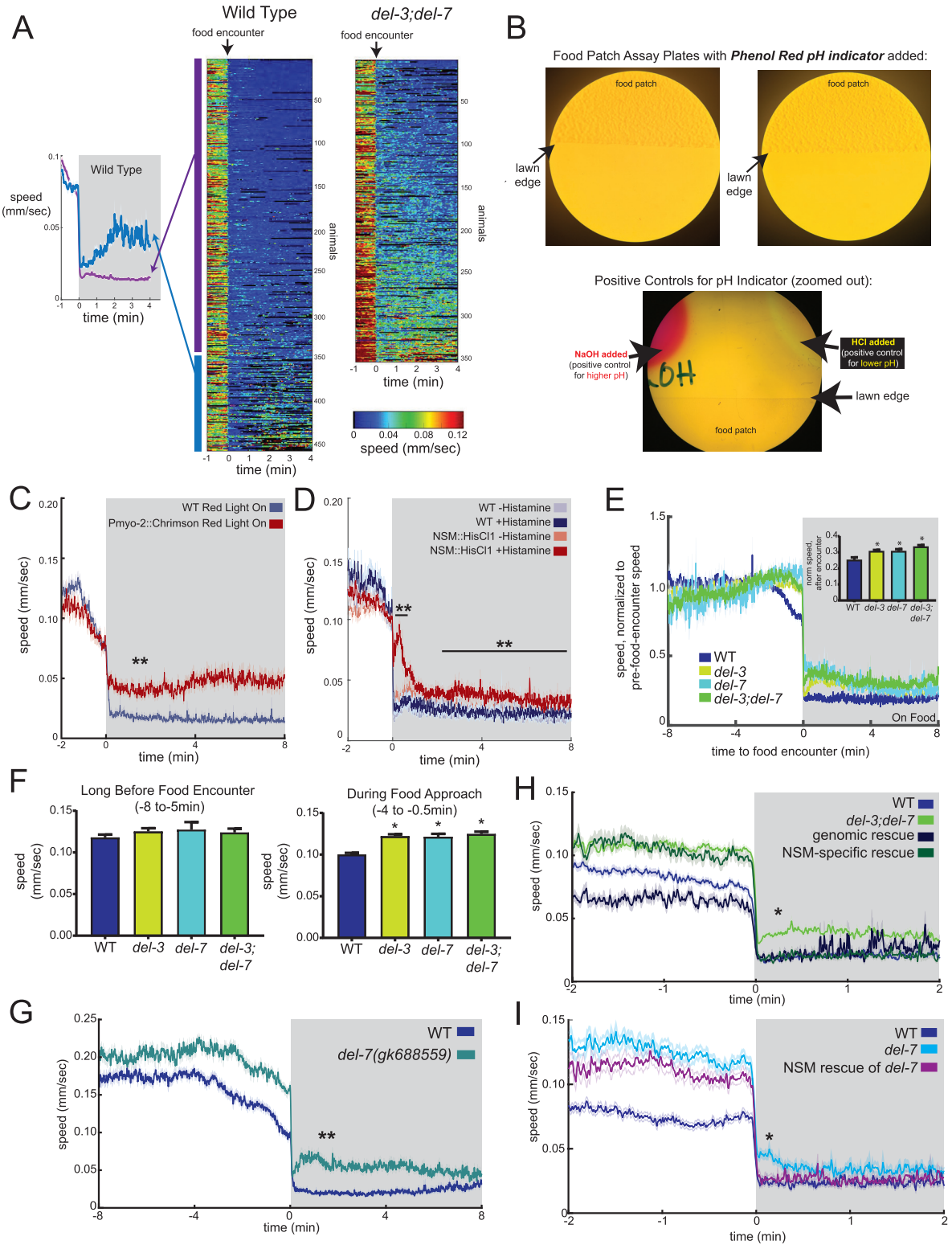

Figure S4. Experiments to Clarify Behavioral Effects during Food Encounters, Related to Figure 4

(A) Heatmaps depicting each animal's speed surrounding food encounters in bacterial food patch assays. Animals are sorted based on average speed after 1min. Average traces (left) show that while some WT animals persistently slow down after encountering food (purple), other WT animals speed back up after 1min (blue). (B) Images of bacterial food patch assay plates with Phenol Red pH indicator dye added. Top: images of two representative food patches. Note that there is no

(legend continued on next page)

detectable change in pH on or near bacterial lawns. Bottom: a food patch assay plate with positive controls for high and low pH also shown. (C) Average speeds of WT and *myo-2::Chrimson* animals encountering food with red light on ($n \geq 63$ animals per condition). *myo-2::Chrimson* animals show significantly less slowing post-encounter (**$p < 0.001$, t test). (D) Average speeds of WT and NSM::HisCl1 animals in the absence or presence of histamine. Silencing NSM via HisCl1 leads to a defect in both initial and persistent behavioral slowing. **$p < 0.001$, ANOVA and Bonferroni-corrected post hoc test. $n \geq 55$ animals per condition. (E) Average speed of the indicated genotypes surrounding food patch encounters, normalized to baseline speed before food encounters (-8 to -0.5 min prior). Inset: average speed values after encounter, from 0-8min (*$p < 0.01$ for two-way ANOVA with *del-3* and *del-7* as two factors). (F) Average animal speed during indicated periods of time, for WT, *del-3*, *del-7* and *del-3;del-7* genotypes (*$p < 0.01$, ANOVA and multiple comparison corrected t test versus N2). (G) Average speeds of WT and *del-7(gk688559)* animals encountering food ($n \geq 56$ animals per condition). *del-7(gk688559)* animals show significantly less slowing (**$p < 0.0001$, t test). (H) Average speeds surrounding food encounters in WT animals and *del-3;del-7* mutants, as well as genomic and NSM-specific cDNA rescues of mutant animals ($n \geq 72$ animals in each condition). Note that expression from genomic fragment rescues speed defects before and after food encounter, whereas NSM-specific expression only rescues post-food-encounter speed (*$p < 0.01$, ANOVA and Bonferroni-corrected t test). (I) Average speeds of animals surrounding food encounters, as in (H). $n > 101$ animals per condition; *$p < 0.01$, ANOVA and multiple comparison corrected t test. Data are shown as means ± SEM.

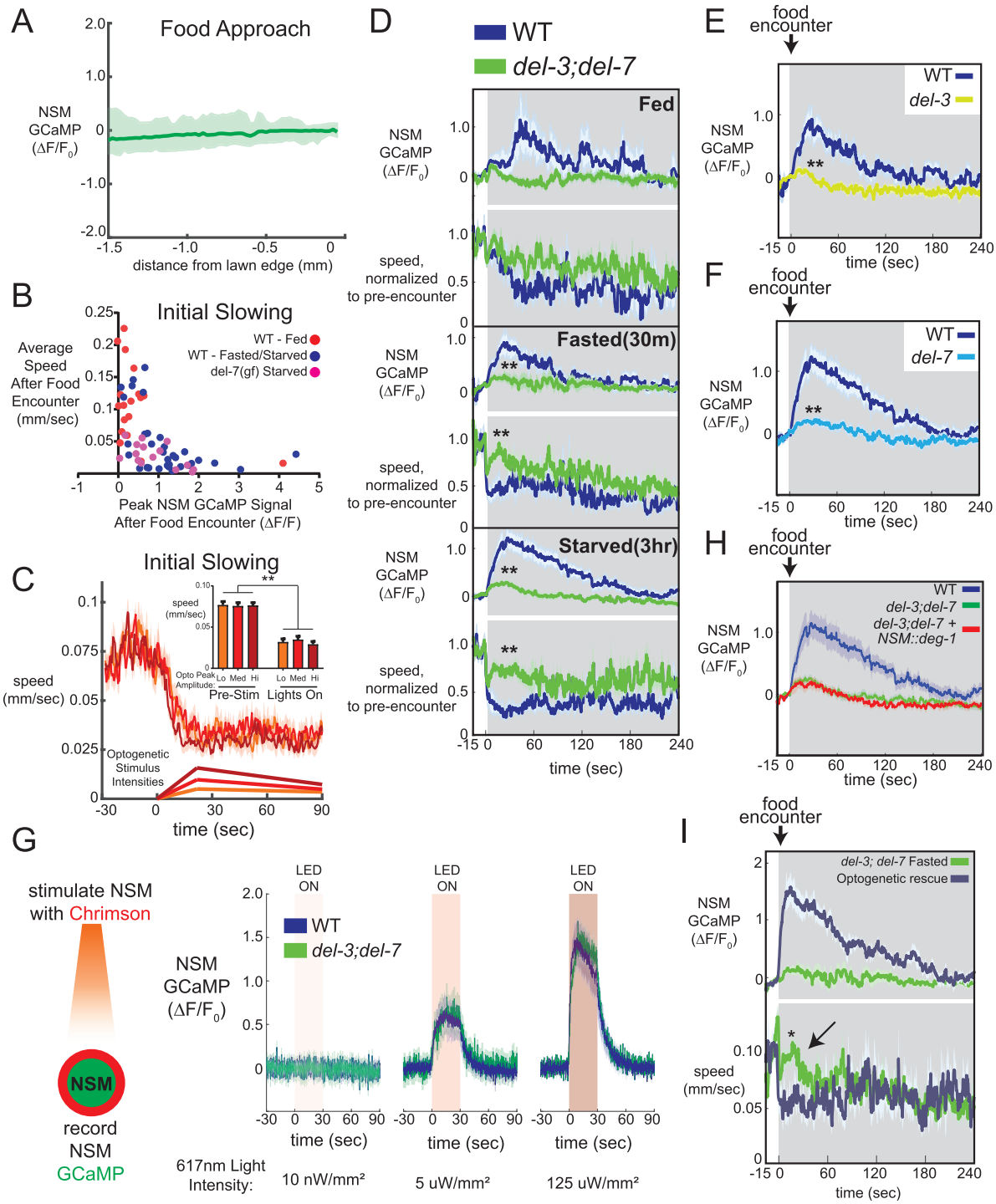

Figure S5. Further Characterization of NSM Activity Patterns, Related to Figure 5

(A) NSM activity does not change during the approach to a bacterial food lawn. Data are from 21 WT animals (fasted or starved) that had continuous NSM GCaMP data for at least 1.5mm preceding encounter with the food lawn. Data are shown as medians with error shade reflecting 10th and 90th deciles. (B) Scatterplot relating individual animals' NSM GCaMP responses immediately after food encounter to their average speed immediately after food encounter. Note the "L" shaped distribution of data points. (C) Optogenetic activation of NSM on food at varying light intensities induces the same magnitude speed reduction in the first 90sec. Inset: Summary data for all animals. N ≥ 51 animals per condition and **p < 0.0001, ANOVA and multiple comparison corrected pairwise test. (D) Average NSM GCaMP and animal speed data for the indicated genotypes in fed, fasted (30 m), or starved (3hr) conditions surrounding food patch encounters. Data are from same animals in Figure 5E, but here the speed data are normalized to pre-food-encounter levels. **p < 0.01, t test for speed or p < 0.01, Mann Whitney test for

(legend continued on next page)

maximum NSM peak value. (E) Average NSM GCaMP for WT and *del-3* mutant animals after 30 m fasting during food patch encounters. n ≥ 21 animals per condition, **p < 0.01, t test. (F) Average NSM GCaMP for WT and *del-7* mutant animals after 3hr starvation during food patch encounters. n ≥ 20 animals per condition, **p < 0.01, t test. (G) Average NSM GCaMP traces from non-feeding, immobilized WT and *del-3;del-7* mutant animals, where NSM was stimulated with Chrimson at three different light intensities. Note there is no difference between WT and *del-3;del-7* animals at any light level. 10 animals per genotype; each animal stimulated twice at each light intensity (thus, n = 20 per condition). (H) Average NSM GCaMP for WT, *del-7;del-3*, and *del-7;del-3* with *NSM::deg-1* expression during food patch encounters. n ≥ 20 animals per condition. (I) Average NSM GCaMP for fasted *del-7;del-3* animals and *del-7;del-3* animals with optogenetic activation of NSM applied at the time of food patch encounters. n ≥ 11 animals per condition. *p < 0.05, ANOVA and multiple comparison-corrected t test. Summary data are shown in Figure 5H. For C-I, data are shown as means ± SEM.

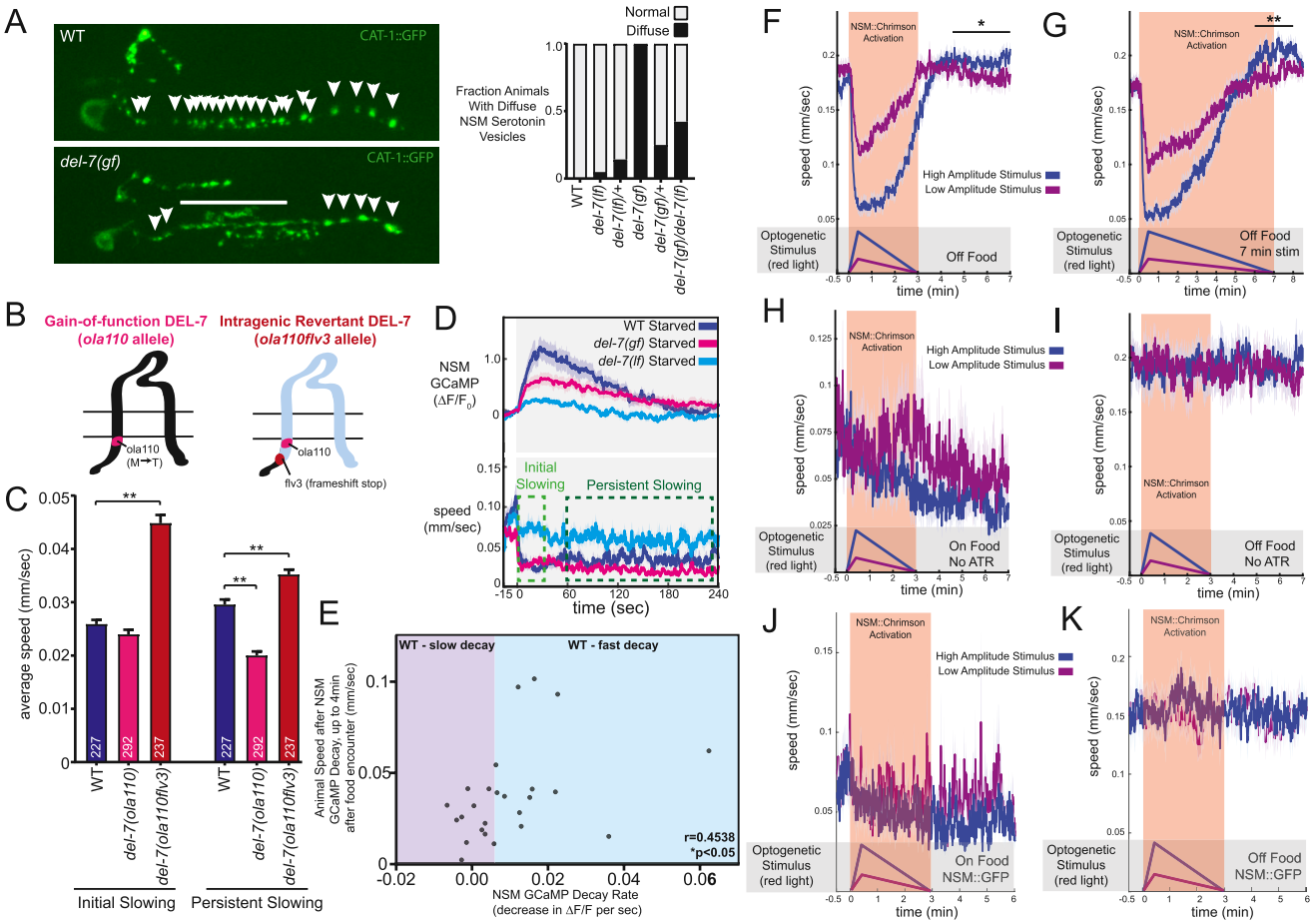

Figure S6. Controls and Other Conditions Related to *del-7*(*ola110gf*) Allele and Optogenetic Manipulation of NSM, Related to Figure 6

(A) Left: representative images of CAT-1::GFP distribution in WT and *del-7(ola110gf)* animals. Arrowheads indicate vesicle clusters. Note diffuse distribution of synaptic vesicles in *del-7(ola110gf)* indicated by bar. Right: NSM CAT-1::GFP vesicle distribution in the indicated genotypes. Each animal was scored as having normal (punctate) CAT-1::GFP distribution or diffuse CAT-1::GFP distribution. n ≥ 18 animals per condition. (B) Cartoons depicting the *del-7(ola110)* gain-of-function, and *del-7(ola110flv3)* intragenic revertant alleles. (C) Average speed of the indicated genotypes immediately after food encounter (first 30 s after encounter) or minutes after encounter. **p < 0.01, ANOVA and multiple-comparison corrected pairwise test. (D) Average NSM GCaMP and animal speed for the indicated genotypes surrounding food patch encounters. Note that *del-7(gf)* and *del-7(lf)* alleles differ in their GCaMP and speed changes in response to food. n ≥ 20 in each condition. (E) Scatterplot showing individual WT animals' NSM GCaMP decay rate and average speed after NSM GCaMP decays. Note the positive correlation across data points (Spearman r = 0.4538, p < 0.05). (F-K) Average speed of *del-7;del-3* animals in response to high (blue) or low (purple) amplitude optogenetic activation of NSM. Data are shown as means ± SEM (F-G) Animals are stimulated off food for (F) 3 minutes (n ≥ 100 animals per condition; *p < 0.05, t test) or (G) 7 minutes (n ≥ 112 animals per condition; **p < 0.01, t test). (H-I) Animals that were not fed all-trans-retinal are stimulated on or off food, respectively. (J-K) Animals that were fed all-trans-retinal but express NSM::GFP in place of NSM::Chrimson were stimulated on or off food, respectively.